UPPER MANTLE STRUCTURE DEDUCED FROM SEISMIC RECORDS ACQUIRED DURING PROJECT EDZOE IN SOUTHERN SASKATCHEWAN AND WESTERN MANITOBA BETWEEN DISTANCES OF ABOUT 790 KILOMETERS AND 1285 KILOMETERS

A Thesis Presented to the
Faculty of Graduate Studies and Research
of
The University of Manitoba

In partial fulfillment
of the requirements for the degree
Master of Science

by
Allan Clifford Bates
March, 1971

TABLE OF CONTENTS

LIST OF TABLES

LIST OF FIGURES

ABSTRACT

In August 1969, the Seismology Division of the Dominion Observatory detonated a series of chemical explosions in Greenbush Lake, British Columbia; the project is known as "Project Edzoe". A total of twenty explosions were attempted in 180 feet of water. The seismic field crew from the Department of Earth Sciences, University of Manitoba, obtained eight seismic records along an east-west profile in southern Saskatchewan and Manitoba; recording distances were in the range 790 to 1285 kilometers.

Signal frequencies on the records were less than 7 Hz; noise frequencies were generally above 7 Hz. Analog playbacks increased the signal to noise ratio by about 68 percent; digital filters offered no improvement over analog playbacks.

An upper mantle velocity structure consisting of a linear velocity-depth gradient, below the base of the crust, accounts for first arrival times. However, uncertainty of crustal structure beneath the shot point and recording sites produces uncertainty in the velocity at the base of the crust and the velocity gradient immediately below it. A second arrival, following the first within about one second, can be explained by a rapid increase in velocity gradient

occurring between depths of about 120 and 150 kilometers. Evidence is given for the existence of a very low gradient following the rapid increase.

ACKNOWLEDGEMENTS

I am grateful to Dr. D. H. Hall for his valuable guidance and discussions during the entire course of the project.

I would like to thank Dr. K. S. Burke for his advice prior to the commencement of the project.

I am indebted to Dr. Z. Hajnal for his patient explanations of digital filtering aspects.

I wish to thank the Standard Oil (Indiana) Foundation for financial assistance during the academic year.

I would also like to thank Mr. J. Wishart and Mr. G. Friesen for their assistance on the field crew.

CHAPTER I

INTRODUCTION

In August 1969, the Seismology Division of the Dominion Observatory detonated a series of chemical explosions in Greenbush Lake, British Columbia. The purpose of the explosions was to assist Canadian and U.S. universities and government agencies to carry out crustal and upper mantle investigations. A total of 20 explosions were attempted in 180 feet of water. A single component instrument was maintained at Lumby, 88 kilometers from the shot point. The project is called "Project Edzoe".

The seismic field crew from the Department of Earth Sciences, University of Manitoba, successfully obtained eight seismic records along an east-west profile in southern Saskatchewan and Manitoba. The recording equipment, which includes the Texas Instruments Incorporated VLF-2 refraction system, is described by Hajnal (1970). The recording stations have been given the names S1 to S8. Figure 1 shows the locations of the shot point and recording sites; Fig. 2 shows the recording site geometry. Locations and distances of the recording sites, and times, charge weights and amplitudes at Lumby of the corresponding shots are given in Table I. Locations and distances of recording sites are given for

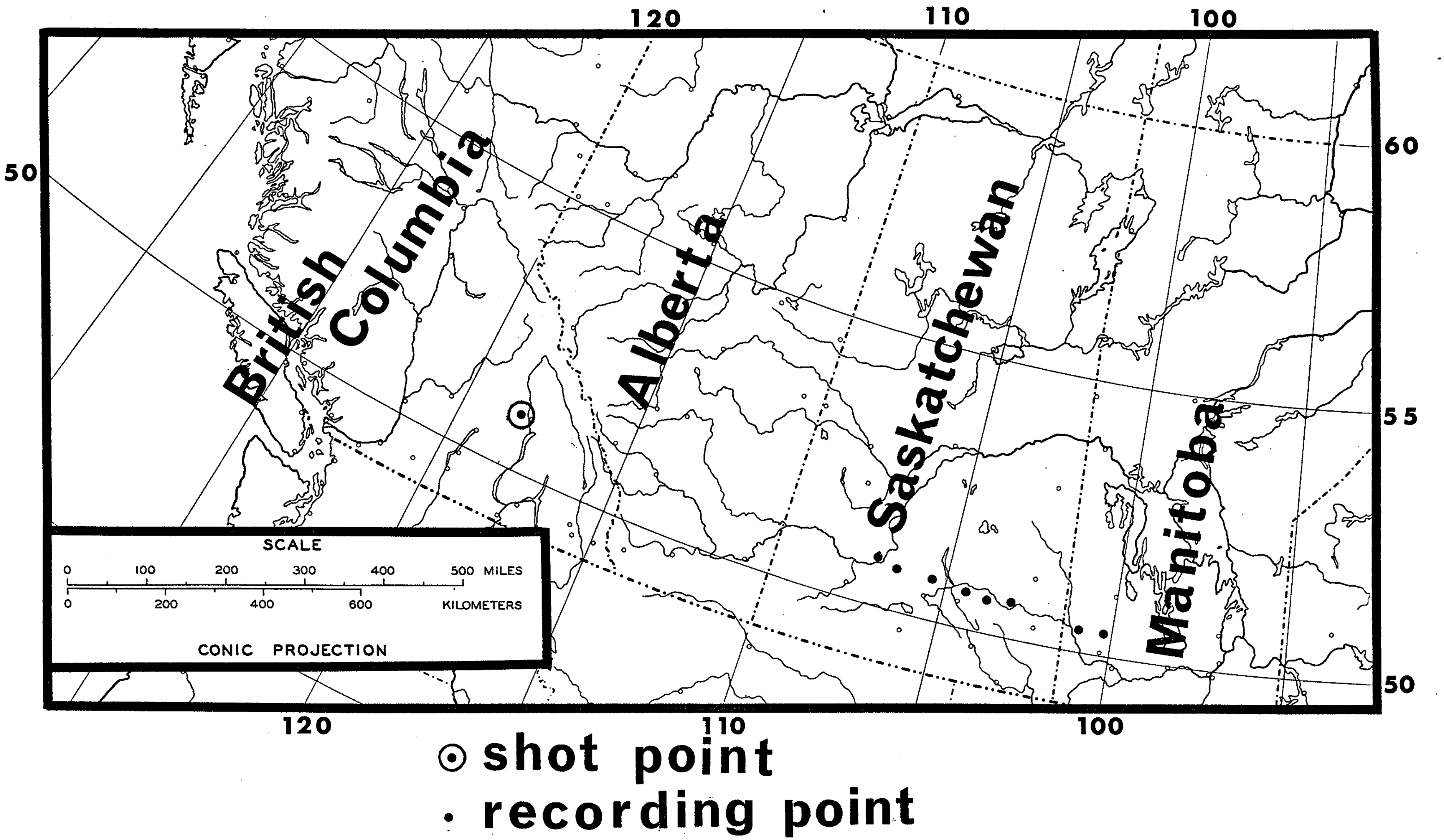

Fig. 1. Location map.

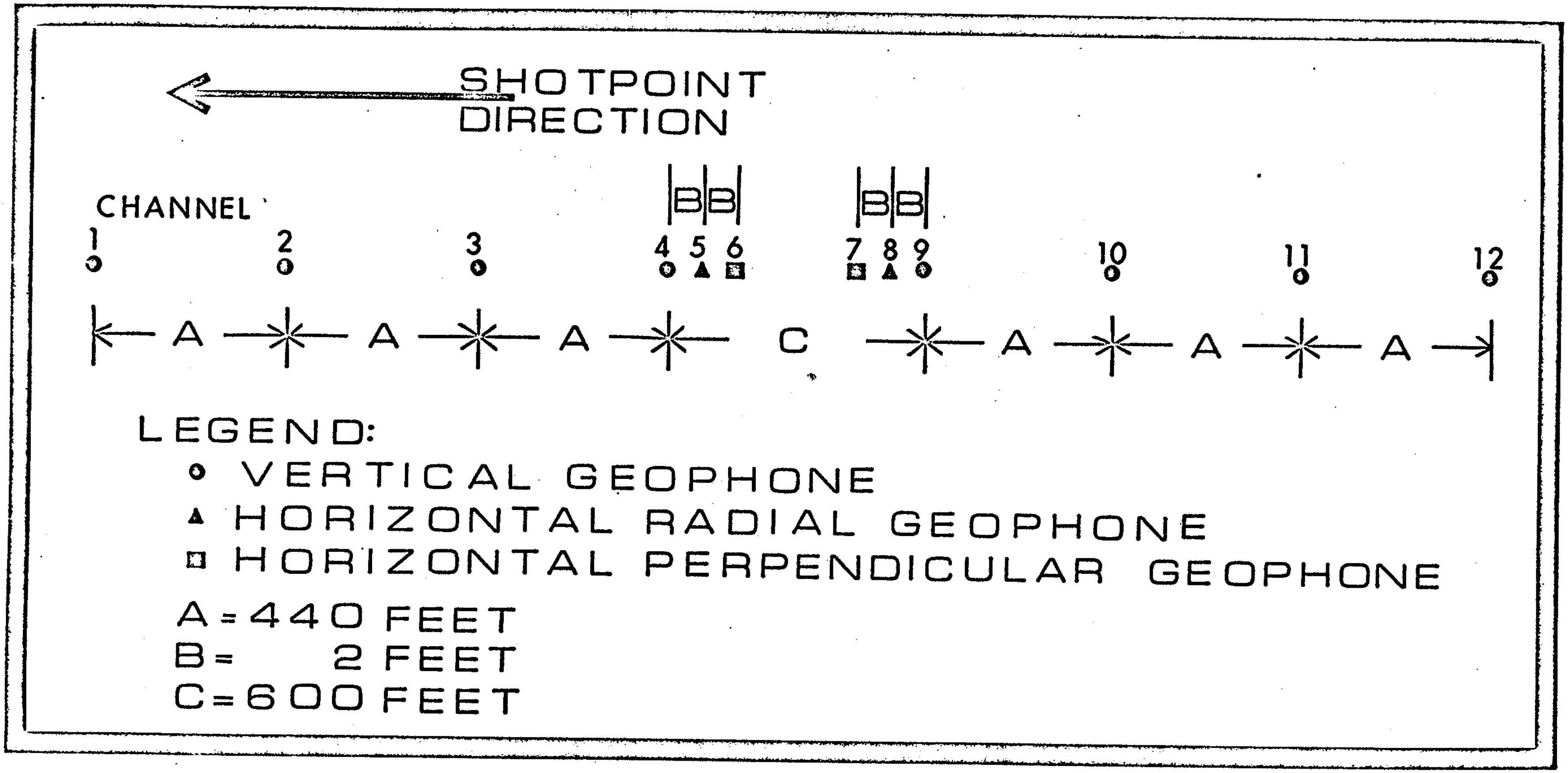

Fig. 2. Recording site geometry.

Table I

Shot Point and Recording Site Information

Shot Point Located at 50° 46.90 ± 0.03'N
118° 20.66 ± 0.06'W

Recording Station	Location	Distance (kilometers)	Shot Date	Shot Time GMT	Charge (pounds minol)	Amplitude at Lumby (relative)
S1	50° 51.55±0.1'N 107° 4.68±0.1'W	793.2±0.3	Aug.15,1969	07:05:00.17	13,293	2
S2	50° 47.23±0.1'N 106° 33.26±0.1'W	830.6±0.3	Aug.17,1969	07:05:00.17	13,293	9½
S3	50° 46.37±0.1'N 105° 34.54±0.1'W	898.4±0.3	Aug.16,1969	07:05:00.17	13,293	8
S4	50° 41.02±0.1'N 104° 26.76±0.1'W	979.9±0.3	Aug.18,1969	07:05:00.16	13,293	8½
S5	50° 37.65±0.1'N 103° 44.25±0.1'W	1030.4±0.3	Aug.19,1969	07:05:00.17	13,293	8½
S6	50° 38.74±0.1'N 103° 1.15±0.1'W	1080.6±0.3	Aug.20,1969	07:05:00.15	13,293	9
S7	50° 23.02±0.1'N 100° 57.47±0.1'W	1229.4±0.3	Aug.22,1969	07:05:00.17	12,660	8½
S8	50° 17.85±0.1'N 100° 11.92±0.1'W	1284.3±0.3	Aug.23,1969	07:05:00.17	13,293	7½

geophone (channel) 1. The shot corresponding to record S1 was a partial misfire due to improper priming. Distances were determined from Fortran program "1 Origin Many Locations" kindly provided by the Department of Physics, University of Alberta. The program computes distances on the basis of the 1924 international constants for the reference ellipsoid (International Dictionary of Geophysics, 1967).

CHAPTER II

SEISMIC FILTERS

The purpose of this chapter is to give bases of description of seismic filters and to describe existing filtering techniques on these bases.

Bases of Description of Seismic Filters

1. The purpose of any seismic filter is to extract signal from a seismic record consisting of signal plus noise. The observer defines those seismic events which are signal and those which are noise. Once signal and noise are defined, a seismic filter is accordingly defined. Thus, filtering techniques are described in terms of the definition of signal and noise.
2. The general filtering method is also a basis of description. General filtering methods include physical, mathematical or digital, and electronic methods.
3. The specific filtering method applied is the final basis of description. This part of the description includes exact mathematical, electronic or physical details of the technique.

Glossary of Seismic Filtering Techniques

Following is a description of several, but by no means all, filtering techniques which are presently employed in seismology.

Array wavelength filter: a physical deconvolution filter. Seismic events of a specified wavelength are rejected by means of suitable shotpoint-detector geometry. Usually Rayleigh and Love waves are considered to be noise. Holzman (1963) describes how Chebyshev polynomials may furnish optimum shot-detector geometries for given problems. Roden (1965) applies wavelength filtering to teleseisms.

Deconvolution filter: a filter which performs the inverse process of any of the filtering processes resulting from the passage of seismic energy through the earth. Deconvolution is equivalent to the commonly used term 'inverse convolution'. Rice (1962) discusses a mathematical approach to inverse convolution filters.

Frequency band-pass filter: a filter which accepts those seismic events within a certain frequency range and rejects those events which are outside of this range. This type of filter is effective when there is a marked separation between signal and noise frequencies. Frequency filters may be electrical or digital.

Laser beam filtering: is effective in removing both coherent noise and incoherent noise from a seismic variable density record. Velocity and frequency filtering by means of laser beam are discussed by Dobrin *et al.* (1965, 1967).

Motion product filter: a physical filter which combines voltages of a three component seismometer in order to suppress random noises arriving from all directions. White (1964) describes such a filter.

Multichannel filter: a filter which acts on more than one trace of a seismic record. Any multichannel filter inherently uses redundancy as a noise reducing mechanism.

Multiple reflection deconvolution filter: (also called "Ghost Elimination Filter") a deconvolution filter which separates primary reflections (signal) from multiple reflection (noise). Lindsey (1960) discusses the realization of such a filter by means of an analog feedback system. Goupillaud (1961) uses a direct approach to filtering multiples. Hammond (1962) describes a physical ghost elimination filter. Silverman *et al.* (1963) approach the problem of multiples by means of "Murac", an analog computer. Schneider *et al.* (1965) combine multichannel digital filtering with stacking to remove primary reflections from multiples plus noise. Anstey *et al.* (1966) show the effectiveness of sectional auto-correlograms and sectional retro-correlograms in separating primary and multiple reflections.

Non-linear filter: a filter designed for non-stationary time series input. Robinson (1967) presents non-linear filter theory. Clarke (1968) describes time varying deconvolution filters.

Optimum filter: a filter which is designed on the basis of some optimality condition; because of complexities generally encountered as a result of the optimality conditions, optimum filters are usually digital.

Predictive filter: a filter which removes random events from a seismic record by predicting future values of a given stationary stochastic process. Usually predictive filters are Wiener filters; the prediction operator is calculated such that the predicted output is as close as possible (in the least squares sense) to a particular desired output. Predictive filters are described in detail by Robinson(1967).

Predictive deconvolution filter: a predictive filter which removes undesirable seismic energy responses caused by the earth. Discussion is given by Robinson (1967).

Recursive filter: a filter which produces output which is a function of both input and past output values. The term "recursive" is used when the filter is digital; an electrical recursive filter is called a feedback filter. Meyerhoff (1966) describes a combination stacking and optimum feedback system. Shanks (1967) gives a general discussion of recursive filters. Usually recursive filters are computationally efficient.

Stacking filter: a filter which removes random noise by means of simple addition of several seismic traces. The terms "multiple coverage" and "common depth (reflection) point" are associated with the stacking technique; channels representing common reflection points are stacked to remove random noise. Stacking filters are more effective than frequency filters when there is an overlap in signal and noise frequencies, however, they are not designed for the removal of coherent noise. Stacking filters are discussed by Mayne (1962) and Galbraith *et al.* (1968).

Velocity filter: a deconvolution filter which accepts all seismic events within a specified apparent velocity band and rejects seismic events outside of this band. Thus noise of frequency and wavelength, which fall in the signal frequency and wavelength range, may often be removed on the basis of apparent velocity separation. A fan filter is a velocity filter which passes events that have apparent velocities which fall within a certain fan-shaped region in the frequency-wavenumber plane. The "pie-slice" filter described by Embree *et al.* (1963) is another example of a velocity filter.

Wiener filter: an optimum filter. The optimality condition is that the actual output be as close as possible to some specified desired output (in the least squares sense). Wiener filtering is described by Wiener (1949) and Robinson (1967).

Names which have been given to filtering techniques in the literature have been derived on the basis of either broad or specific characteristics of the technique. As a result of this, any specific filter may have a combination of titles. An example of this is the "optimum multichannel velocity deconvolution filter" described by Sengbush *et al.* (1968).

CHAPTER III

FILTERING TECHNIQUES EMPLOYED

Signal frequencies are below 7 Hz and noise frequencies are generally above 7 Hz on the records from the present experiment. Digital and analog filtering were used in an attempt to remove white noise from the records; it was found that digital filtering offered no advantages over simple analog playback filtering.

Digital Filtering

Analog to digital conversion was carried out by means of the Radiation Inc. A/D converter. All twelve channels were digitized for each record. The digitizing interval used was 1.71 milliseconds; hence, the aliasing frequency was about 300 Hz, which is well above signal frequencies. The Radiation converter is described in detail by Hajnal (1970). All digital processing was done on the IBM 360/65 at the Department of Computer Science, University of Manitoba. Digital seismic data was plotted by means of the Calcomp 750/563 plotting system.

Multichannel Digital Prediction Filtering

Multichannel digital prediction filtering was attempted by means of Fortan computer programs written by Burgess (1969). The programs are based on the mathematical theory of prediction described by Robinson (1967). Basically, the program package written by Burgess consists of: "predict 1", a program which computes a general multichannel least squares Wiener filter; and "mftconv", a subroutine which performs multichannel convolution of this filter with segmented input. The eight vertical traces on a few sample seismic records were processed by this technique. Results were unsuccessful; the normalized prediction error of realizable length optimum filters was approximately 0.7. A large prediction error in this case could be attributed to the fact that there were not enough traces (only eight) to comprise a sufficient multichannel stationary random process.

In any event, this multichannel prediction technique is designed for the prediction of first arrivals only.

Low-pass Digital Filtering

A digital seismic filter Fortran program package has been written for the Department of Earth Sciences, University of Manitoba, by Hajnal (1970). Programs within this package used were:

Bandpass: a program which computes weighting coefficients of a bandpass filter and determines the frequency response of the computed filter.

Convolv: filters the seismic data with a set of weighting coefficients calculated by "bandpass".

Plotmod: prepares seismic data for plotting.

The bandpass filter computed by "bandpass" has weighting coefficients, b_t, defined by

$$b_t = \frac{1}{t}\{\sin[2\pi(h+f_o)t] - \sin[2\pi(h-f_o)t]\}(1 - \frac{|t|}{n})$$

$$-n < t < +n \qquad \ldots(3\cdot1)$$

where,

f_o = center frequency of ideal bandpass filter.

h = half-width of ideal bandpass filter.

$(1 - \frac{t}{n})$ = Fejer weighting factor.

t = time.

Figure 3 shows the frequency response curves of digital low-pass filters F_1, F_2, F_3, F_4, described in Table II. An increase in length from 100 to 200 results in a marked improvement in frequency response for both (0-5) Hz and (0-10) Hz filters.

Figure 3 suggests that F_4 would be effective in increasing the signal to noise ratio of the seismic data. Figures 4 and 5 show record S5 unfiltered and filtered with F_4 respectively. The signal to noise ratio of the unfiltered record is approximately 1.6; the signal to noise ratio of the F_4 filtered record is approximately 2.7. Thus, the signal to noise ratio is increased by about 68 percent.

There is a certain ambiguity in the definition of the signal frequency band. Even though each seismic phase consists of frequencies of 7 Hz or less, the superposition of two or more seismic phases contains small wavelets of

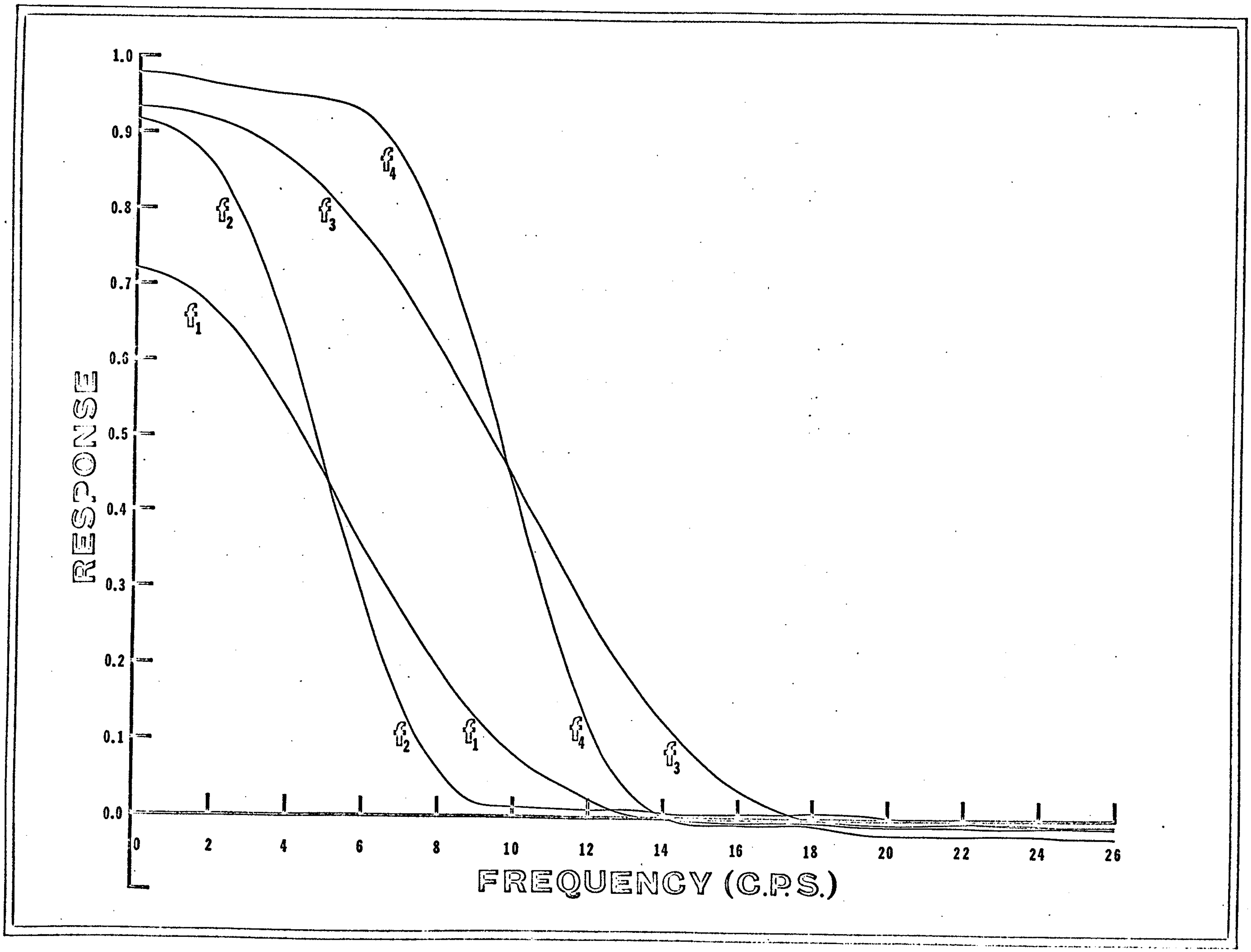

Fig. 3. Frequency response of digital filters F_1, F_2, F_3, F_4.

Table II

Description of Filters F_1, F_2, F_3, F_4

Filter	Low Cut Frequency (Hz)	High Cut Frequency (Hz)	Length of Filter (Number of Samples)
F_1	0	5	100
F_2	0	5	200
F_3	0	10	100
F_4	0	10	200

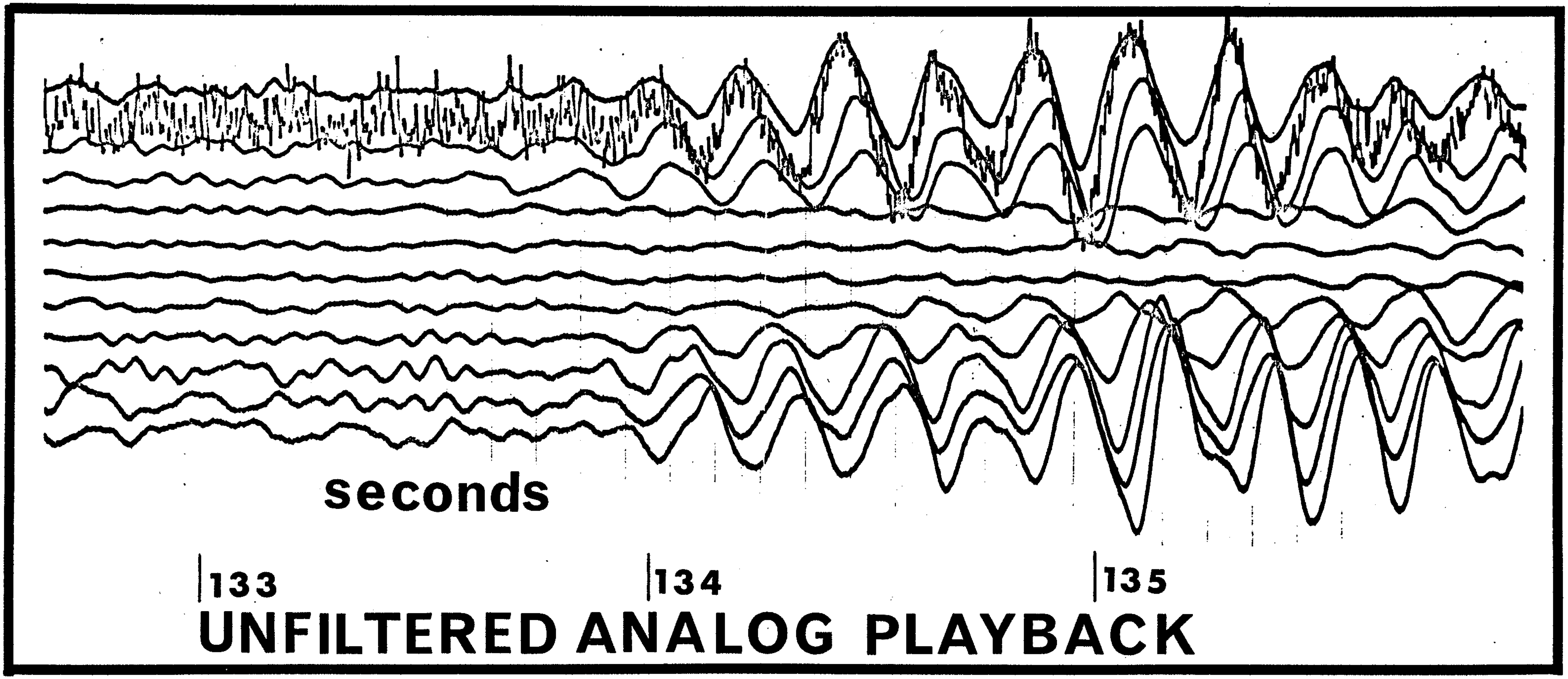

Fig. 4. Record S5 (Playback).

Attenuation (dB)

Channel	1	2	3	4	5	6	7	8	9	10	11	12
Field Record	24	24	24	24	24	24	24	24	24	24	24	24
Playback	48	48	48	48	54	54	54	54	48	48	48	48

Frequency Setting for Field Record = 16 c.p.s.

Frequency Setting for Playback = 48 c.p.s.

leaf 18 ommitted in page numbering

frequency as high as 12 Hz. Small interference wavelets are valuable in determining the onset of seismic phases. In view of this fact, it was necessary to have a compromising low-pass filter which would remove a sufficient amount of noise and leave a sufficient amplitude of wavelets such that the net effect would be the production of readable seismic records. Filter F_4 is such a compromise.

Despite the fact that good digitally filtered records can be obtained with existing programs, "convolv" has disadvantages. The seismic data are stored on tape in the form of 1202 two-byte words. The first two words of a block identify the record and block numbers; the other 1200 words consist of 100 samples from each of the 12 seismic channels (0.171 seconds of seismic information per channel). During the convolution process, five blocks of data are read into core at a time (this is about 0.885 seconds of seismic information per channel). Thus, when it is desirable to process large amounts of data (25 seconds or more), "convolv" becomes input-output bound. Furthermore, "convolv" performs convolution in the time domain, and this is a slow process. In present form, "convolv" uses about 75 minutes CPU time to process 25 seconds of seismic data for twelve channels, a digitizing rate of 1.710 milliseconds, and a filter of length 200. Thus, for large amounts of data, "convolv" is also CPU bound.

The efficiency of "convolv" could be increased by,

1. decreasing the digitizing rate,
2. decreasing filter length,
3. performing convolution in the frequency domain with the fast Fourier transform method described by Robinson (1967).

Analog Filtering

Figure 6 shows the frequency response characteristics of the VLF-2 system. The curve for 8 Hz is very similar to the curve which describes filter F_4 in Fig 3. Figure 11e is an (0-8 Hz) analog playback of record S5; this is to be compared with record S5 filtered with digital low-pass filter F_4 (Fig. 5). Very good results were obtained with (0-8 Hz) analog playbacks; thus, it was not necessary to use digital filtering. Figures 11a to 11h are the (0-8 Hz) analog playbacks of records S1 to S8.

For long range refraction experiments, signal frequencies are very low; the VLF-2 system is designed for such experiments. Digital bandpass filtering would be an improvement over analog playback filtering for studies such as near vertical reflection experiments, in which signal frequencies are higher. In cases such as these, severe limitations are placed on the analog playback system. Hajnal (1970) shows vast improvements by digital filtering techniques on near vertical reflection records.

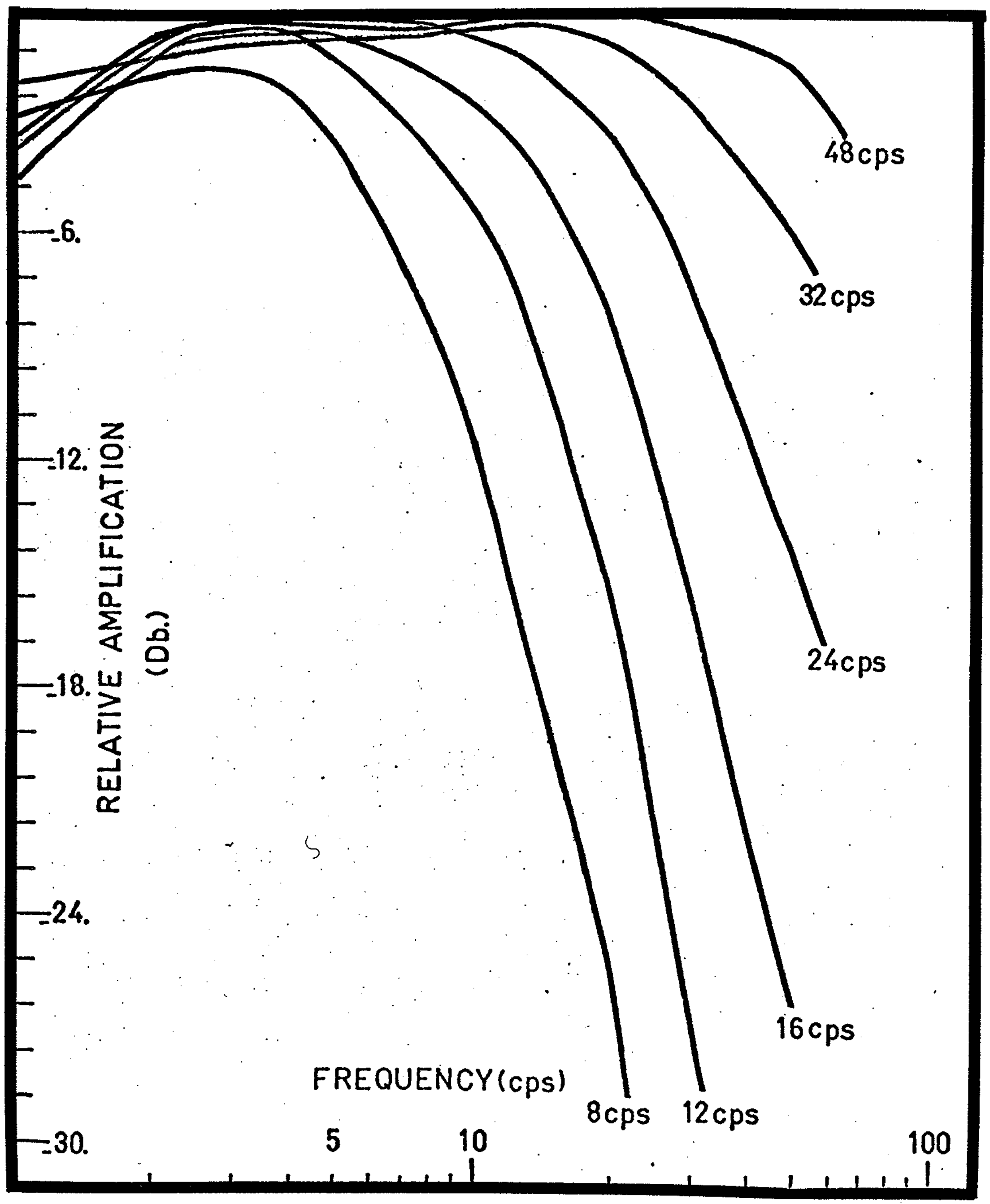

Fig. 6. Frequency response of the VLF-2 refraction system.

CHAPTER IV

INTERPRETATION

An interpretation of the first two arrivals P_1 and P_2, is given in this chapter. Both arrival were found to be the result of rays which penetrate the upper mantle. Unfortunately, no detailed information about the crustal structure under the shot point and recording sites has been published. Uncertainty of crustal structure resulted in uncertainty in mantle structure deduced from mantle arrivals. P_1 and P_2 are shown on the records in Figs. 11a to 11h.

Determination of Upper Mantle Velocity from First Arrival Times

For the distance range of this experiment, rays which penetrate the upper mantle emerge as first arrivals. To account for observed first arrival times, upper mantle linear velocity-depth functions of the form given by equation 4·1 were considered.

$$V_p = V_m \; , \; Z = Z_m$$

$$V_p = V_m + M(Z - Z_m) \, , \quad Z \geq Z_m \; , \; M \geq 0 \qquad \ldots (4 \cdot 1)$$

where

V_p = P wave velocity

V_m = velocity at the base of the crust

Z_m = depth to the base of the crust

M = linear velocity-depth gradient in the upper mantle (seconds^{-1})

Ranges of acceptable values of V_m , the velocity at the base of the crust, and M, the upper mantle gradient, depend upon not only the actual first arrival times, but also the choice of crustal structure and required accuracy of travel times.

Uncertainty in Crustal Structure

Despite the fact that there is no detailed crustal information, it is still possible to restrict the crustal structure to certain ranges. McConnell and McTaggert-Cowan (1963) have calculated the mean crustal velocity and depth to Moho for shields and stable interior platforms (Table III). A range of crustal velocities, 6.34 ± 0.27 km/sec, and crustal thicknesses, 41.06 ± 7.78 kilometers, produces a range in crustal delay times associated with rays which travel through the upper mantle. Acceptable values of V_m and M were determined for the following crustal models:

Crustal Model A; velocity = mean = 6.34 km/sec

crustal thickness = mean = 41.06 km

This model produces an average crustal delay time.

Table III

Mean Crustal Structure for Shields and Stable Interior Platforms (McConnell and McTaggart-Cowan, 1963)

	Crustal Velocity (km/sec)	Crustal Thickness (km)
Mean	6.34	41.06
Standard Deviation	0.27	7.78

Crustal Model B; velocity = mean - standard deviation

= 6.07 km/sec

crustal thickness = mean + standard deviation

= 48.84 km

This model produces a maximum delay time.

Crustal Model C; velocity = mean + standard deviation

= 6.61 km/sec

crustal thickness = mean - standard deviation

= 33.28 km

This model results in a minimum delay time.

Determination of V_m and M

Allowable ranges of V_m and M for a given crustal model and a specified accuracy of arrival times were determined by examining the normalized root mean square error function, E_1, defined by:

$$E_1 = \sqrt{\frac{\sum_{i=1}^{N} (T_i - t_i)^2}{N}}$$

where

T_i = theoretical first arrival time at the i^{th} station

t_i = observed first arrival time at the i^{th} station

N = number of stations at which the first arrival is observed = 8

For a chosen crustal model, E_1 is clearly a function of V_m and M only, since each t_i is a constant. A minimum in the function $E_1(V_m, M)$ occurs when,

$$\frac{\partial E_1}{\partial V_m} = \frac{\partial E_1}{\partial M} = 0 \qquad \ldots(4\cdot2)$$

and corresponds to optimum values (in the least squares sense) of V_m and M. $E_1(V_m, M)$ could possibly be written as an explicit function of V_m and M; optimum values of V_m and M could then be determined by solving equation 4·2. However, since the parametric equations relating time and distance for a spherical geometry and linear velocity-depth functions are very complicated, calculations have been performed using the IBM 360/65 computer.

Table IV shows calculated values of E_1 (seconds^{-1}) for various values of V_m and M, assuming the average crustal model A; the table shows trends in the function E_1. For each of the values of V_m between 7.90 and 8.10, there is a value of M between 0.0005 and 0.007 which corresponds to a minimum in E_1. For $V_m = 8.15$ and $V_m = 8.20$, the table suggests a minimum in E_1 will be found for M less than 0.0005. For each of the values of M between 0.0005 and 0.006 there is a value of V_m between 7.90 and 8.20 which corresponds to a minimum in E_1. For M = 0.007 a minimum will occur when V_m is less than 7.90.

The scanning grid of (V_m, M) values in Table IV is neither fine enough nor extensive enough to determine acceptable solutions for a given error; the purpose of the table is to show the general nature of the error function E_1.

Table IV

Error Function, E_1, for Crustal Model A (Values of E_1 Given in sec)

V_m (km/sec) / M (sec^{-1})	7.90	7.95	8.00	8.05	8.10	8.15	8.20
0.0005	3.30	2.57	1.85	1.15	0.49	0.38	1.00
0.001	3.15	2.42	1.71	1.01	0.36	0.48	1.13
0.002	2.75	2.03	1.32	0.64	0.25	0.83	1.50
0.003	2.22	1.52	0.83	0.32	0.69	1.34	2.01
0.004	1.60	0.95	0.50	0.75	1.35	1.99	2.65
0.005	1.03	0.71	0.96	1.51	2.13	2.77	3.41
0.006	1.00	1.30	1.82	2.41	3.03	3.65	4.28
0.007	1.74	2.25	2.81	3.41	4.02	4.64	5.27

The error function has been calculated with a grid spacing of $\Delta V_m = 0.02$ km/sec and $\Delta M = 0.0001$ seconds^{-1} for each of crustal models A, B and C.

Table V shows the results for crustal model A. For each value of V_m, values of E_1 are given for the range of M which shows E_1 passing through a minimum. Each value of V_m has a minimum value of E_1 which corresponds to an optimum M. The set of minimum values of E_1 also has a minimum; this is shown in Table VI. It should be noted that the minimum value of E_1 for $V_m = 8.14$ km/sec, $V_m = 8.16$ km/sec, and $V_m = 8.18$ km/sec has been taken as the value corresponding to $M = 0$, since negative gradients have not been considered.

In accordance with Table VI, the minimum value of E_1 for any V_m less than 7.98 km/sec must be greater than 0.57 seconds and the minimum value of E_1 for any V_m greater than 8.18 km/sec must be greater than 0.65 seconds. Table V furnishes acceptable values of V_m and M for a given error in observed arrival times (assuming crustal model A).

For each crustal model acceptable values of V_m of the form,

$$V_a \leq V_m \leq V_b$$

were found for first arrival time accuracies of 0.50 seconds and 0.30 seconds. For each value of V_m between V_a and V_b

Table V

Error Function $E_1(V_m, M)$ for Crustal Model A

Grid Spacing: V_m = 0.02 km/sec, M = 0.0001 sec^{-1}

V_m=7.98 km/sec		V_m=8.00 km/sec		V_m=8.02 km/sec		V_m=8.04 km/sec		V_m=8.06 km/sec		V_m=8.08 km/sec	
M (sec^{-1})	E_1 (sec)	M (sec^{-1})	E_1 (sec)	M (sec^{-1})	E_1 (sec)	M (sec^{-1})	E_1 (sec)	M (sec^{-1})	E_1 (sec)	M (sec^{-1})	E_1 (sec)
0.0041	.60	0.0038	.51	0.0031	.54	0.0026	.51	0.0020	.51	0.0013	.51
0.0042	.58	0.0039	.50	0.0032	.50	0.0027	.47	0.0021	.47	0.0014	.48
0.0043	.57	0.0040	.50	0.0033	.47	0.0028	.44	0.0022	.43	0.0015	.44
0.0044	.58	0.0041	.51	0.0034	.45	0.0029	.40	0.0023	.39	0.0016	.41
0.0045	.59	0.0042	.52	0.0035	.43	0.0030	.38	0.0024	.36	0.0017	.38
				0.0036	.42	0.0031	.36	0.0025	.33	0.0018	.34
				0.0037	.43	0.0032	.35	0.0026	.31	0.0019	.31
				0.0038	.44	0.0033	.36	0.0027	.29	0.0020	.29
				0.0039	.47	0.0034	.37	0.0028	.29	0.0021	.26
				0.0040	.51	0.0035	.40	0.0029	.30	0.0022	.25
						0.0036	.44	0.0030	.32	0.0023	.24
						0.0037	.48	0.0031	.35	0.0024	.25
						0.0038	.53	0.0032	.39	0.0025	.27
								0.0033	.43	0.0026	.29
								0.0034	.48	0.0027	.33
								0.0035	.54	0.0028	.37
										0.0029	.41
										0.0030	.46
										0.0031	.52

Table V (continued)

V_m=8.10 km/sec		V_m=8.12 km/sec		V_m=8.14 km/sec		V_m=8.16 km/sec		V_m=8.18 km/sec	
M (sec^{-1})	E_1 (sec)	M (sec^{-1})	E_1 (sec)	M (sec^{-1})	E_1 (sec)	M (sec^{-1})	E_1 (sec)	M (sec^{-1})	E_1 (sec)
0.0004	.51	0	.36	0	.27	0	.41	0	.65
0.0005	.49	0.0001	.35	0.0001	.27	0.0001	.43	0.0001	.66
0.0006	.46	0.0002	.33	0.0002	.27	0.0002	.44	0.0002	.68
0.0007	.44	0.0003	.32	0.0003	.28	0.0003	.45		
0.0008	.41	0.0004	.30	0.0004	.28	0.0004	.47		
0.0009	.39	0.0005	.29	0.0005	.29	0.0005	.49		
0.0010	.36	0.0006	.27	0.0006	.30	0.0006	.51		
0.0011	.34	0.0007	.26	0.0007	.31				
0.0012	.31	0.0008	.25	0.0008	.33				
0.0013	.29	0.0009	.24	0.0009	.35				
0.0014	.26	0.0010	.23	0.0010	.37				
0.0015	.25	0.0011	.23	0.0011	.39				
0.0016	.23	0.0012	.24	0.0012	.42				
0.0017	.22	0.0013	.25	0.0013	.44				
0.0018	.22	0.0014	.26	0.0014	.47				
0.0019	.23	0.0015	.28	0.0015	.51				
0.0020	.25	0.0016	.31						
0.0021	.28	0.0017	.34						
0.0022	.31	0.0018	.37						
0.0023	.35	0.0019	.41						
0.0024	.39	0.0020	.45						
0.0025	.43	0.0021	.49						
0.0026	.48	0.0022	.53						
0.0027	.53								

Table VI

Minimum Value of E_1 for Each V_m

(Crustal Model A)

V_m (km/sec)	7.98	8.00	8.02	8.04	8.06	8.08	8.10	8.12	8.14	8.16	8.18
Minimum Value of E_1 (sec)	0.57	0.50	0.42	0.35	0.29	0.24	0.22	0.23	0.27	0.41	0.65

there is an acceptable range of M of the form,

$$M_a \leq M \leq M_b \ , \ M_a \geq 0$$

Table VII lists V_a and V_b for the three crustal models. Table VIII gives M_a and M_b corresponding to acceptable values of V_m. For a given crustal model, acceptable values of V_m which are lower have higher values of M. Crustal model A represents an average crustal delay time; accordingly, solution values of V_m and M are intermediate. Crustal model B represents a maximum delay time; high values of V_m and low values of M are required for a solution. Crustal model C represents a minimum delay time; low values of V_m and high values of M are required.

The effect of crustal structure upon the solution of upper mantle velocity is more easily seen by comparing the best solutions of V_m and M for each crustal structure. Solutions A, B and C are the best solutions of V_m and M assuming crustal structures A, B and C respectively;

Solution A: V_m = 8.10 km/sec, M = 0.0017 sec^{-1},
E_1 = 0.22 sec

Solution B: V_m = 8.32 km/sec, M = 0 sec^{-1},
E_1 = 0.37 sec

Solution C: V_m = 7.88 km/sec, M = 0.0036 sec^{-1},
E_1 = 0.27 sec

Figure 7 shows solutions A, B and C graphically. Table IX lists theoretical and observed first arrival times, and

Table VII

Solutions of V_m, $V_a \leq V_m \leq V_b$

for Crustal Models A, B, and C

Crustal Model	Accuracy of First Arrival Times (sec)	V_a (km/sec)	V_b (km/sec)
A	.50	8.00	8.16
	.30	8.06	8.14
B	.50	8.28	8.34
	.30	- No Solutions	-
C	.50	7.80	7.96
	.30	7.86	7.90

Table VIII

Solutions of M, $M_a \leq M \leq M_b$, for First

Arrival Time Accuracies of 0.5 sec and 0.3 sec

Crustal Model A

	0.5 sec Accuracy		0.3 sec Accuracy	
V_m (km/sec)	M_a (sec^{-1})	M_b (sec^{-1})	M_a (sec^{-1})	M_b (sec^{-1})
8.00	0.0039	0.0040	-	-
8.02	0.0032	0.0039	-	-
8.04	0.0027	0.0037	-	-
8.06	0.0021	0.0034	0.0027	0.0029
8.08	0.0014	0.0030	0.0020	0.0026
8.10	0.0005	0.0026	0.0013	0.0021
8.12	0	0.0021	0.0004	0.0015
8.14	0	0.0014	0	0.0006
8.16	0	0.0005	-	-

Table VIII (Continued)

Crustal Model B

V_m (km/sec)	0.5 sec Accuracy M_a (sec^{-1})	0.5 sec Accuracy M_b (sec^{-1})	0.3 sec Accuracy M_a (sec^{-1})	0.3 sec Accuracy M_b (sec^{-1})
8.28	0.0010	0.0017	-	-
8.30	0	0.0014	-	-
8.32	0	0.0009	-	-
8.34	0	0.0002	-	-

Crustal Model C

V_m (km/sec)	0.5 sec Accuracy M_a (sec^{-1})	0.5 sec Accuracy M_b (sec^{-1})	0.3 sec Accuracy M_a (sec^{-1})	0.3 sec Accuracy M_b (sec^{-1})
7.80	0.0047	0.0052	-	-
7.82	0.0043	0.0050	-	-
7.84	0.0039	0.0047	-	-
7.86	0.0035	0.0044	0.0039	0.0041
7.88	0.0031	0.0041	0.0035	0.0038
7.90	0.0027	0.0038	0.0031	0.0033
7.92	0.0022	0.0033	-	-
7.94	0.0018	0.0028	-	-
7.96	0.0014	0.0022	-	-

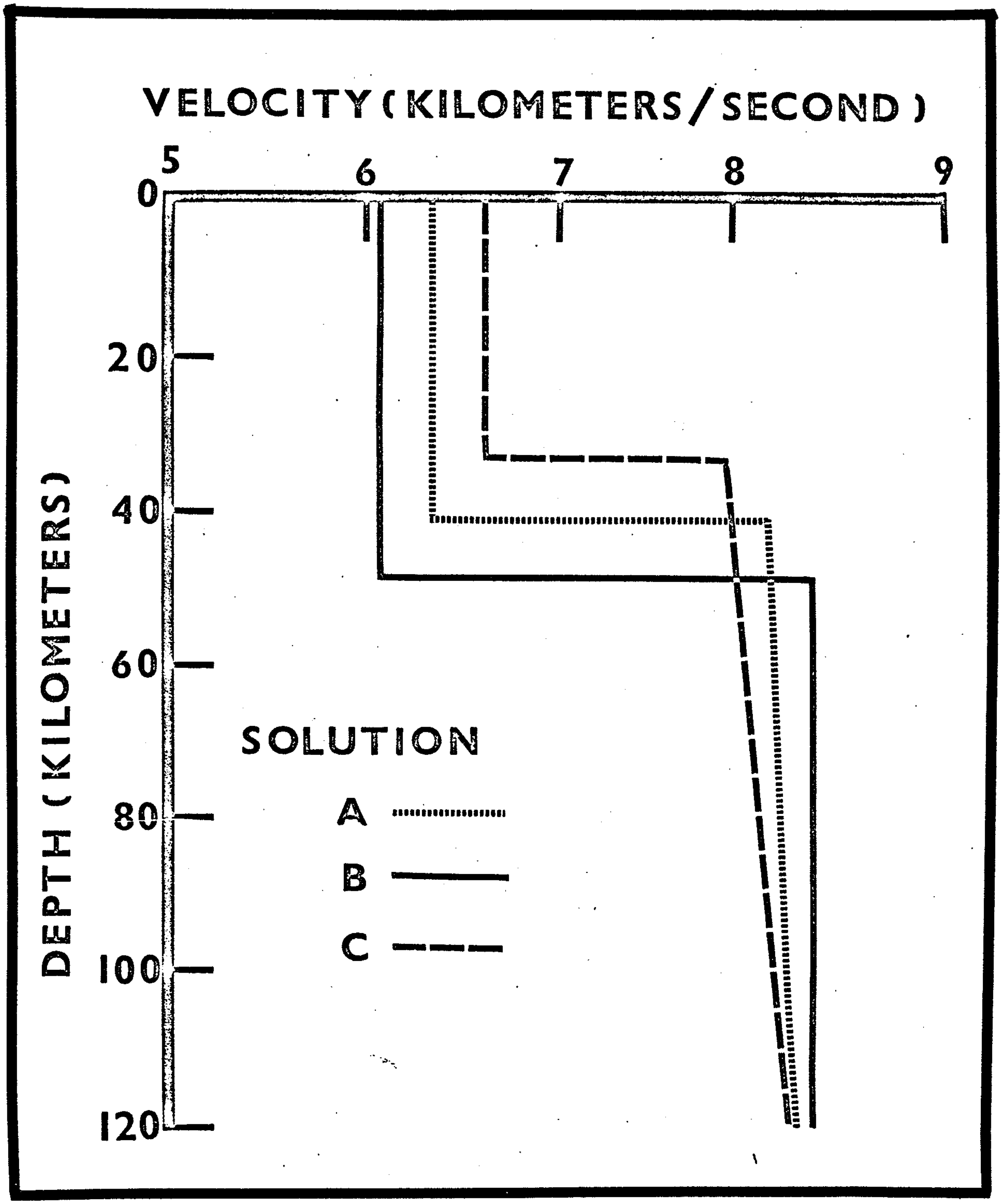

Fig. 7. Best solutions for crustal models A, B, and C.

Table IX

Theoretical First Arrival Times and Depth of Penetration of Rays for Best Solutions A, B, and C

Station	Distance (km)	Actual First Arrival Time (sec)	Theoretical First Arrival Time (sec)			Depth of Penetration of Ray Emerging (km)		
			Solution A	Solution B	Solution C	Solution A	Solution B	Solution C
S1	793.2	105.38	105.17	105.62	105.00	62.8	54.2	70.0
S2	830.6	109.54	109.72	110.07	109.61	65.2	54.7	74.2
S3	898.4	118.12	117.96	118.14	117.94	69.9	57.0	82.0
S4	979.9	127.78	127.84	127.84	127.89	76.1	59.7	92.5
S5	1030.4	133.86	133.95	133.86	134.03	80.3	61.4	99.4
S6	1080.6	139.60	140.01	139.82	140.11	84.6	63.4	106.7
S7	1229.4	158.25	157.93	157.51	157.95	98.8	69.4	130.4
S8	1284.3	164.40	164.51	164.03	164.46	104.6	72.0	139.9

depths of penetration of rays which emerge at the recording sites for solutions A, B and C. The range in depth at which the rays bottom depends drastically upon the choice of crustal structure.

The velocity at the base of the crust, and the velocity gradient within the upper mantle cannot be determined accurately on the basis of first arrival times. Uncertainty of crustal structure permits a wide range of values for V_m and M, even when observed first arrival times are known to an accuracy of ±0.30 seconds (Table VIII). However, the velocity-depth functions corresponding to the best solutions for a wide range of crustal structures (A, B and C) do converge with depth as shown in Fig. 7.

Evidence of Upper Mantle Velocity Structure from Second Arrivals

A second event, P_2, has been picked on all of the records except S1 which is of poor quality. On record S2, P_2 has been taken as the third energy arrival since the arrival time of the second event does not correlate with arrival times of P_2 on the other records.

The possibility that P_2 is either a multiple reflection at the free surface or a PS conversion has been eliminated.

Green and Hales (1968) have reported strong multiple phases (PP, PPP and PPPP) on seismic records from Project Early Rise. They point out that, theoretically, these phases should not be visible for the distances at which they have observed them. For a velocity of 6 km/sec in the upper part of the crust, P_2 arrives too early to be a conventional multiple reflection.

The PS converted wave is composed of SV type motion. It results from the conversion of energy, in the form of a refraction, from the parent P wave at the interface between two crustal layers of contrasting seismic velocity. Schwind *et al.* (1960) find various multiple PS conversions on seismic records up to about 400 kilometers. However, amplitude curves of McCamy *et al.* (1962) show that the ratio of converted PS wave amplitude to parent P wave amplitude is very small for distances of this experiment. For example, for a conversion at a boundary separated by seismic P wave velocities of 6.0 km/sec and 6.5 km/sec, the amplitude ratio is less than 0.05 at a distance of about 1000 kilometers.

Effect of Rapid Increase in Velocity Gradient

A rapid increase in velocity gradient produces a triplication in a time-distance plot (Fig. 8). It was assumed that P_2 was part of a triplication corresponding to branch XY in Fig. 8. Observed arrival times of P_2 were explained by a velocity gradient M_2 commencing at a depth Z_2 such that M_2 was greater than the velocity gradient above Z_2. For each of solutions A, B, and C, upper mantle velocity functions of the following form were considered:

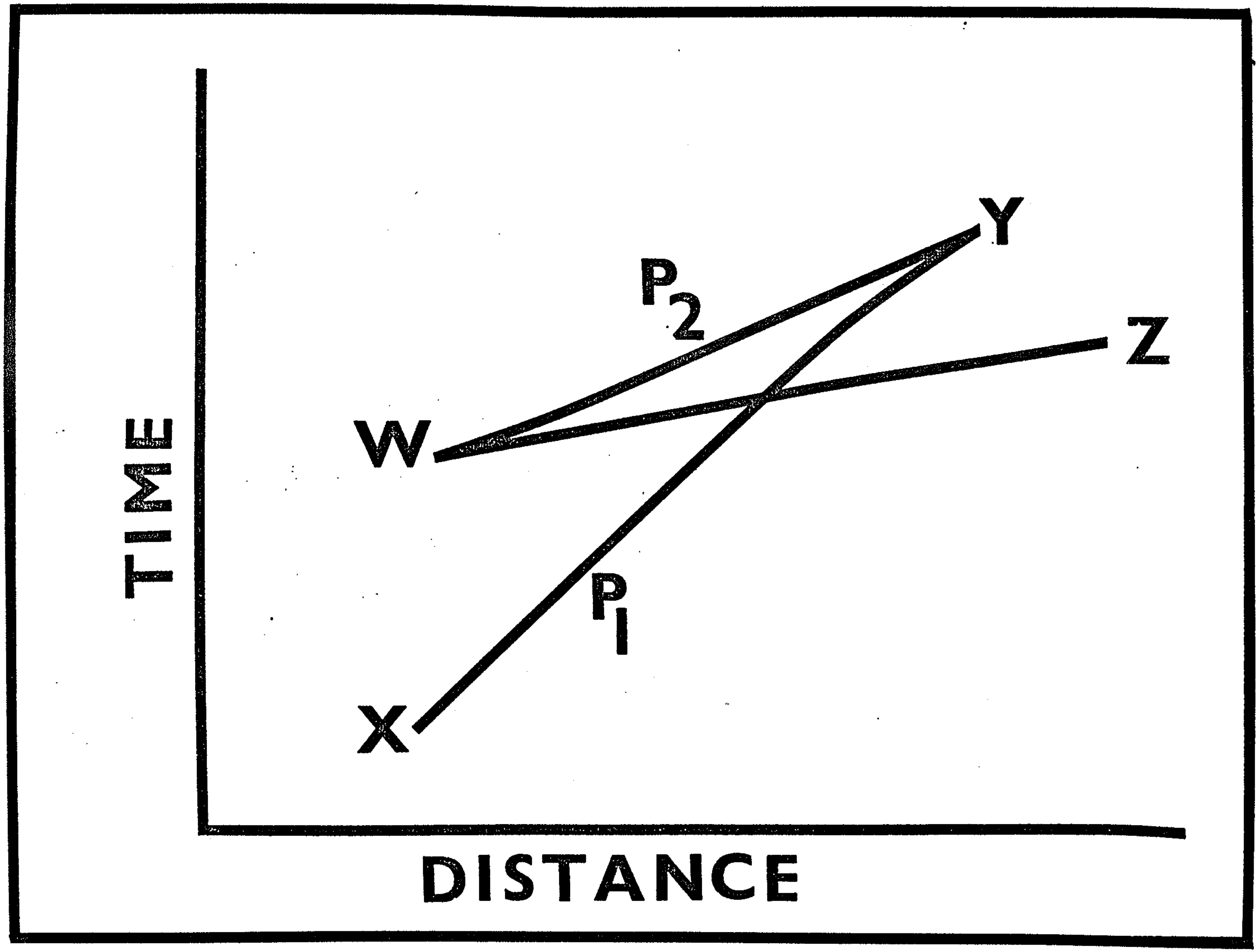

Fig. 8. Triplication

$$V_p = V_1 + M_1(Z - Z_1), \quad Z_2 \geq Z \geq Z_1$$

$$V_p = V_1 + M_1(Z_2 - Z_1) + M_2(Z - Z_2), \quad Z \geq Z_2$$

where

V_p = P wave velocity in upper mantle

(V_1, M_1) = best values (in the least squares sense) of V_m and M for solution A, B or C.

Z = depth

Z_1 = crustal thickness or crustal model corresponding to solution A, B or C

Z_2 = depth at which the velocity gradient becomes M_2

M_2 = new upper mantle gradient such that $M_2 > M_1$

Z_2 and M_2 were restricted to values for which:

i) the point Y, on Fig. 8, occurs at a distance greater than 1284 kilometers (the largest distance at which P_2 is observed).

ii) the point W, on Fig. 8, occurs at a distance less than 831 kilometers (the smallest distance at which P_2 is observed).

For each of solutions A, B and C, a normalized root mean square error function, E_2, was calculated for increments of 10 kilometers in Z_2 and various values of M_2:

$$E_2 = \sqrt{\frac{\sum_{i=2}^{8}(T_i - t_i)^2}{N}}$$

where

T_i = theoretical arrival time of P_2 at the i^{th} station

t_i = observed arrival time of P_2 at the i^{th} station

N = number of stations at which P_2 is observed = 7

The choice of solutions A, B or C (and, in turn, the choice of crustal model A, B or C) allows variation in the depth, Z_2, at which a rapid increase in velocity can take place. Following are the values of Z_2 and M_2 for which E_2 is less than about 0.5 seconds.

Calculations assuming Solution A (Crustal model A):

Z_2 = 120 kilometers, $M_2 > 0.0155 \pm 0.0005$ sec^{-1}

Z_2 = 130 kilometers, $M_2 > 0.0185 \pm 0.0005$ sec^{-1}

Z_2 = 140 kilometers, $M_2 > 0.045 \pm 0.005$ sec^{-1}

Calculations assuming Solution B (Crustal model B):

Z_2 = 120 kilometers, $M_2 > 0.025 \pm 0.005$ sec^{-1}

Calculations assuming Solution C (Crustal model C):

Z_2 = 140 kilometers, $M_2 > 0.0205 \pm 0.0005$ sec^{-1}

Z_2 = 150 kilometers, $M_2 > 0.055 \pm 0.005$ sec^{-1}

The best value of E_2 is about 0.4 sec; it occurs when the average crustal model A is assumed and Z_2 = 130 kilometers, $M_2 > 0.025 \pm 0.005$ sec^{-1}.

P_2/P_1 Amplitude Ratio:

For each of solutions A, B and C, the theoretical P_2/P_1 amplitude ratios, based on geometric spreading, were calculated for values of Z_2 and M_2 for which E_2 is less than about 0.5 seconds. It was found that the P_2/P_1 ratio does not change appreciably with either a change in solution (crustal model) or changes in (Z_2, M_2) values for a given solution (crustal model). Thus, acceptable (Z_2, M_2) values cannot be restricted further on the basis of amplitude ratios. However, the theoretical P_2/P_1 amplitude ratios do show general agreement with observed P_2/P_1 amplitude ratios. Figure 9 shows the theoretical P_2/P_1 ratios for solution A (Z_2 = 130 kilometers, M_2 = 0.10 sec^{-1}) plotted against observed values.

Velocity changes sufficient to explain P_2

It has been shown that P_2 arrival times and P_2/P_1 amplitude ratios can be explained if the velocity gradient suddenly increases between depths of about 120 kilometers and 150 kilometers. The value of the new gradient, M_2, is bounded below but it may tend to infinity. However, M_2 need only exist to a depth Z_3 such that P_2 will theoretically be observed at a distance of about 831 kilometers (the distance of station S2). Table X gives Z_3, $V_p(Z_3)$, and $V_p(Z_2)$ for solutions A, B and C, and for acceptable values of Z_2 and M_2. A linear change of velocity from $V_p(Z_2)$ to $V_p(Z_3)$ between depths of Z_2 and Z_3 is sufficient to explain the existence of the P_2 phase at distances as small as 831 kilometers. For a given solution and a given depth Z_2 at which M_2 begins, clearly Z_3 is a function of M_2 only. Furthermore, $V_p(Z_3)$

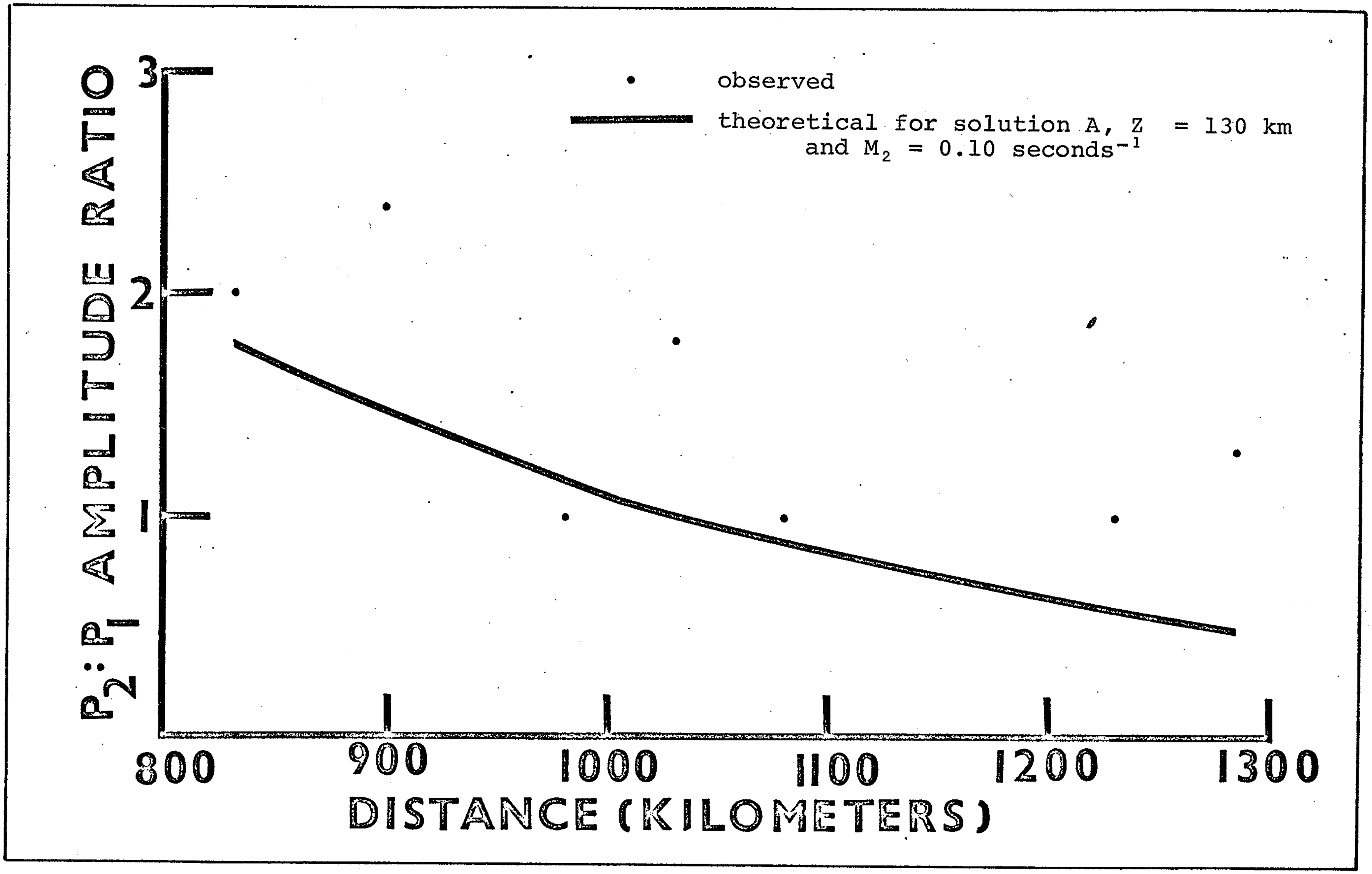

Fig. 9. Theoretical and actual $P_2:P_1$ amplitude ratio.

Table X

Sufficient Depth, Z_3, to which M_2 Must Continue

Calculations Assuming Solution A (Crustal Model A)

Z_2 = 120 km, $V_p(Z_2) = 8.23\ \frac{km}{sec}$			Z_2 = 130 km, $V_p(Z_2) = 8.25\ \frac{km}{sec}$			Z_2 = 140 km, $V_p(Z_2) = 8.27\ \frac{km}{sec}$		
M_2 (sec^{-1})	Z_3 (km)	$V_p(Z_3)$ (km/sec)	M_2 (sec^{-1})	Z_3 (km)	$V_p(Z_3)$ (km/sec)	M_2 (sec^{-1})	Z_3 (km)	$V_p(Z_3)$ (km/sec)
0.016	147.4	8.67	0.019	152.6	8.68	0.05	144.5	8.49
0.02	130.4	8.44	0.03	137.2	8.47	0.1	141.9	8.46
0.03	124.8	8.38	0.05	133.4	8.42	0.2	140.9	8.45
0.1	121.0	8.34	0.1	131.6	8.42	1	140.2	8.44
0.2	120.5	8.33	0.2	130.7	8.38	2	140.1	8.43
1	120.1	8.32	0.3	130.4	8.38	3	140.1	8.43
2	120.0	8.32	1	130.1	8.38	4	140.0	8.43
3	120.0	8.32	2	130.1	8.38	10	140.0	8.43
4	120.0	8.32	3	130.0	8.37			
10	120.0	8.32	10	130.0	8.37			

Table X (Continued)

Calculations Assuming Solution B (Crustal Model B)

Z_2 = 120 km

$V_p(Z_2) = 8.32 \frac{km}{sec}$

M_2 (sec^{-1})	Z_3 (km)	$V_p(Z_3)$ (km/sec)
0.03	125.6	8.49
0.04	123.8	8.47
0.05	122.9	8.46
0.1	121.3	8.45
0.2	120.6	8.44
0.3	120.4	8.44
1	120.1	8.44
2	120.1	8.44
5	120.0	8.44
10	120.0	8.44

Calculations Assuming Solution C (Crustal Model C)

Z_2 = 140 km

$V_p(Z_2) = 8.26 \frac{km}{sec}$

M_2 (sec^{-1})	Z_3 (km)	$V_p(Z_3)$ (km/sec)
0.021	163.7	8.76
0.05	143.5	8.44
0.06	142.7	8.43
0.07	142.2	8.42
0.1	141.4	8.41
0.5	140.3	8.39
1	140.2	8.39
2	140.1	8.38
5	140.0	8.38
10	140.0	8.38

Z_2 = 150 km

$V_p(Z_2) = 8.30 \frac{km}{sec}$

M_2 (sec^{-1})	Z_3 (km)	$V_p(Z_3)$ (km/sec)
0.06	153.6	8.52
0.1	151.9	8.49
0.2	150.9	8.47
0.3	150.6	8.47
0.5	150.3	8.46
1	150.2	8.46
2	150.1	8.46
5	150.0	8.46
10	150.0	8.46

is purely a function of M_2:

$$V_p(Z_3) = V_p(Z_2) + M_2 \times [Z_3(M_2) - Z_2]$$

The physical situation corresponding to the limit as M_2 tends to infinity is a velocity discontinuity, from which P_2 would be a total reflection. Accordingly, from Table X, $\lim_{M_2 \to \infty} Z_3(M_2) = Z_2$ and $\lim_{M_2 \to \infty} V_p(Z_3)$ exists and is greater than $V_p(Z_2)$. For example, for solution A and $Z_2 = 130$ kilometers, $V_p(Z_2) = 8.25$ km/sec and $\lim_{M_2 \to \infty} V_p(Z_3) = 8.37$ km/sec. For the entire range of solutions, the difference between $\lim_{M_2 \to \infty} V_p(Z_3)$ and $V_p(Z_2)$ is as small as 0.09 km/sec and as large as 0.26 km/sec. When $Z_3 - Z_2$ is large, then the difference $V_p(Z_3) - V_p(Z_2)$ is also large. For the entire range of solutions, the P_2 event can be explained by a difference between Z_3 and Z_2 as large as about 25 kilometers and a corresponding difference between $V_p(Z_3)$ and $V_p(Z_2)$ as large as about 0.45 km/sec.

Uncertainty of crustal structure was seen to have a pronounced effect on the determination of the P wave velocity distribution in the upper mantle based on P_1 arrival times. However, determination of deeper velocity structure, based on the P_2 event, is only slightly affected by this uncertainty.

Observed arrival times of P_2 and theoretical P_2 arrival times for solution A, $Z_2 = 130$ kilometers, and $M_2 = 0.03$ sec^{-1} are listed in Table XI.

Table XI

Arrival Times of P_2

(Theoretical arrival times are given for Solution A, $Z_2 = 130$ km, $M_2 = 0.03$ sec^{-1})

Station	Distance (km)	Observed Arrival Time (sec)	Theoretical Arrival Time (sec)
S2	830.6	110.56	111.26
S3	898.4	119.11	119.14
S4	979.9	128.73	128.68
S5	1030.4	134.70	134.62
S6	1080.6	140.61	140.54
S7	1229.4	158.89	158.14
S8	1284.3	165.06	164.65

Incomplete Triplication

P_1 and P_2 have been considered to be part of a triplication (segments WX and XY given in Fig. 8. There is, however, no event, P_3 say, observed on the records which corresponds to segment YZ in Fig. 8. The absence of a P_3 event could be the result of the existence of a low velocity zone below Z_3 or a zone of very low gradient below Z_3. There is no direct evidence for a low velocity layer, but it is feasible that a zone of low gradient could produce a P_3 event of very small amplitude such that it would not be observed. For example, for solution A and $Z_2 = 130$ kilometers, $M_2 = 2.0$ seconds^{-1}, a velocity gradient of 1.0×10^{-6} seconds^{-1}, existing below Z_3, would produce a P_3 event such that the amplitude ratio P_1/P_3 is approximately 4 for all distances of the experiment. The ratio of P_1 amplitude to noise amplitude, as stated in Chapter III, was found to be about 2.7. Thus, the P_3 event would be buried in noise.

Figure 10 is a reduced time-distance plot showing observed values and the theoretical graph for solution A, $Z_2 = 130$ kilometers, and $M_2 = 0.03$ seconds^{-1}.

Other Arrivals

Arrivals, other than P_2, which occur within about 5 seconds after P_1 may be part of minor triplications (Green and Steinhart, 1962). Since the records are of

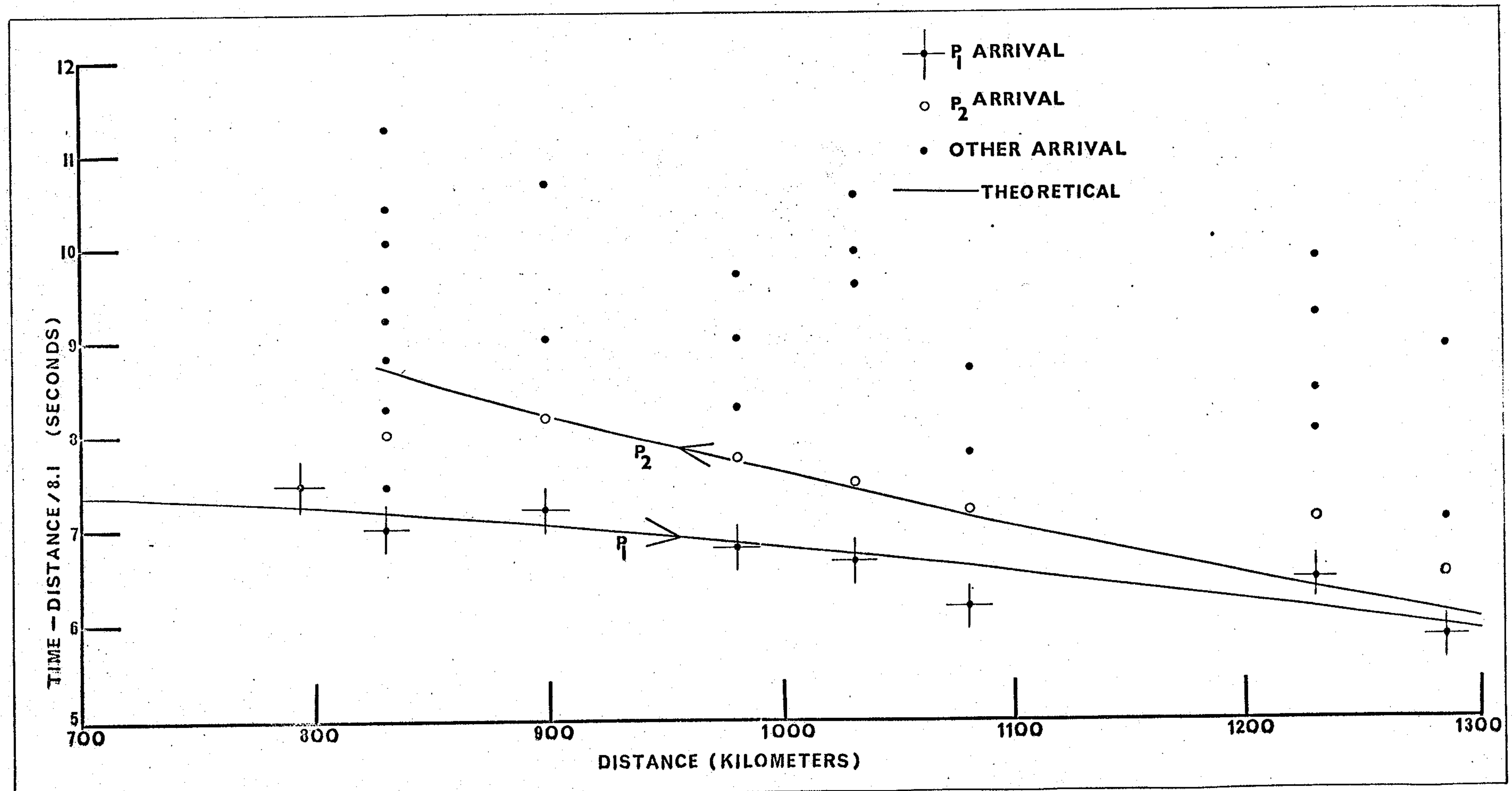

Fig. 10. Reduced time - distance plot; theoretical curve is for Solution A, Z_2 = 130 km, M_2 = 0.03 seconds^{-1}

varying quality and the station spacing is large (up to 150 kilometers), it is difficult to trace events, which may be part of minor triplications, from record to record.

The $\bar{P}$ Phase

The $\bar{P}$ phase is present on all of the records; it is very strong on all records except S8. Figures 12a and 12b show $\bar{P}$ on records S2 and S8 respectively. Velocities and arrival times for the $\bar{P}$ phase are given in Table XII. The velocity given is the distance divided by the arrival time.

The $\bar{P}$ phase arrives at times expected for the direct wave, P_g. However, for distances of this experiment, P_g theoretically should not be visible. The presence of $\bar{P}$ indicates a velocity gradient in the crust.

Results from Project Early Rise

Green and Hales (1968) have interpreted records from Project Early Rise to determine upper mantle structure in the Central United States. Two Early Rise models are proposed. For Model 1, velocity increases slowly below the Moho (50 km depth); a rapid increase in velocity gradient occurs at 89 km (the velocity increases by 0.26 km/sec); below 89 km, the velocity gradient is low. This model is similar in form to the models A, B, and C. Model 2 is similar to Model 1 down to a depth of about 134 km; at this depth Model 2 includes a low velocity layer 25 km thick. However, observations explained by the low velocity layer may also be explained by lateral velocity variation.

Table XII

$\overline{P}$ Phase

Station	Distance (km)	Arrival Time (sec)	Velocity (km/sec)
S1	793.2	131.75	6.02
S2	830.6	138.38	6.00
S3	898.4	149.97	5.99
S4	979.9	164.63	5.95
S5	1030.4	174.03	5.92
S6	1080.6	180.06	6.00
S7	1229.4	207.47	5.93
S8	1284.3	214.65	5.98

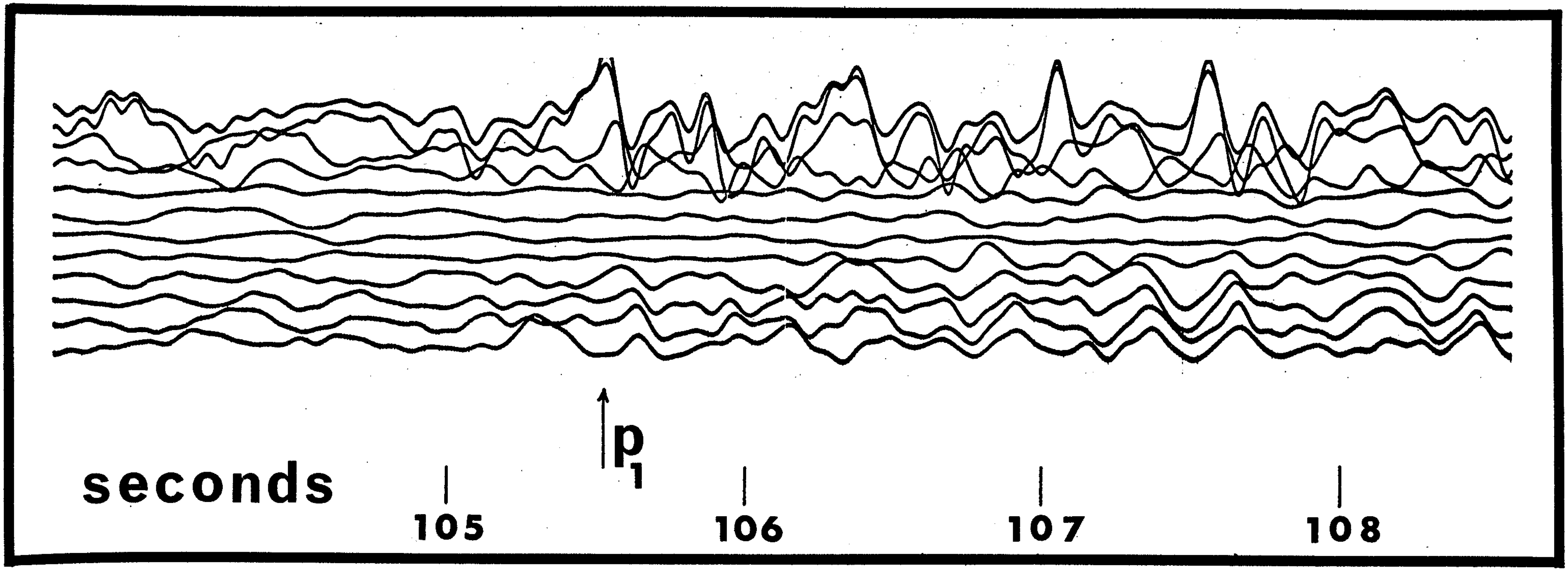

Fig. 11a. Record S1 (Playback). Distance = 793.2 km.

	Attenuation (dB)											
Channel	1	2	3	4	5	6	7	8	9	10	11	12
Field Record	18	18	18	18	24	24	24	24	24	24	24	24
Playback	42	42	42	42	48	48	48	48	42	42	42	42

Frequency Setting for Field Record = 18 c.p.s. (all channels)

Frequency Setting for Playback = 8 c.p.s. (all channels)

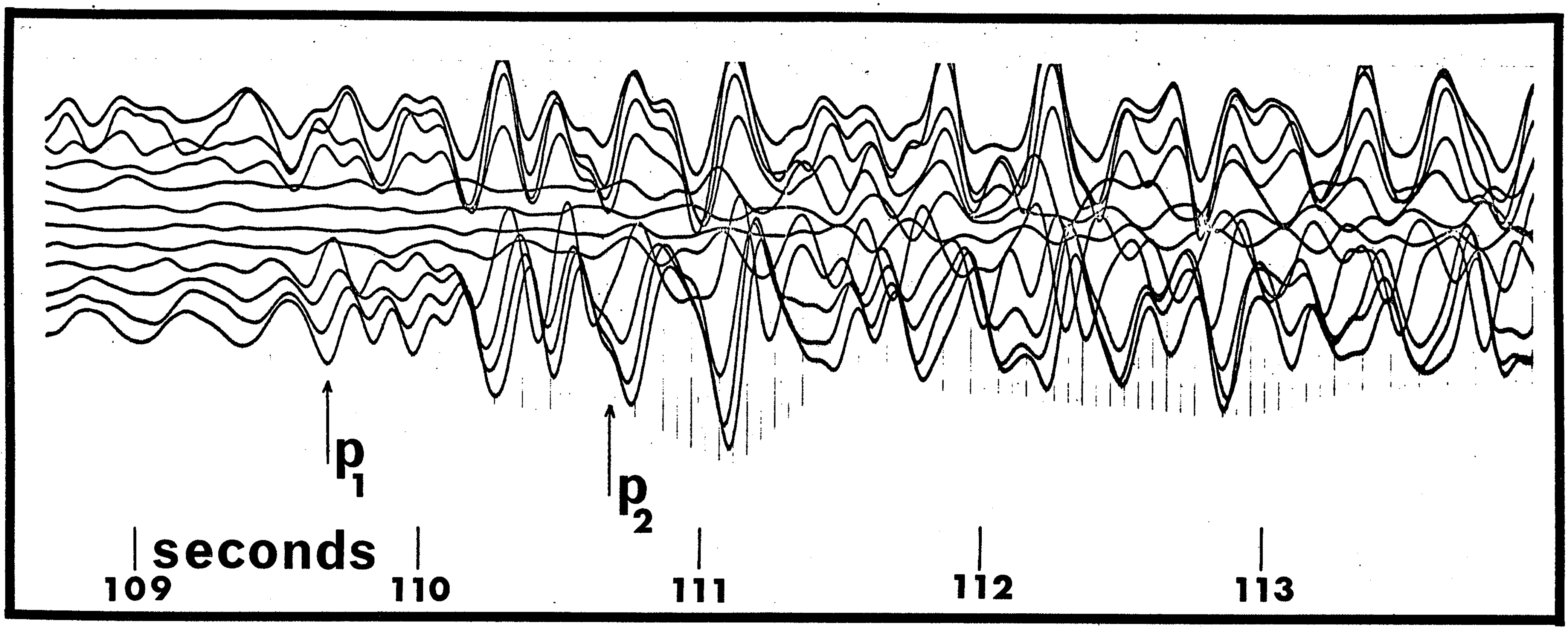

Fig. 11b. Record S2 (Playback). Distance = 830.6 km.

Attenuation (dB)

Channel	1	2	3	4	5	6	7	8	9	10	11	12
Field Record	30	30	30	30	30	30	30	30	30	30	30	30
Playback	42	42	42	42	42	42	42	42	42	42	42	42

Frequency Setting for Field Record = 18 c.p.s. (all channels).

Frequency Setting for Playback = 8 c.p.s. (all channels).

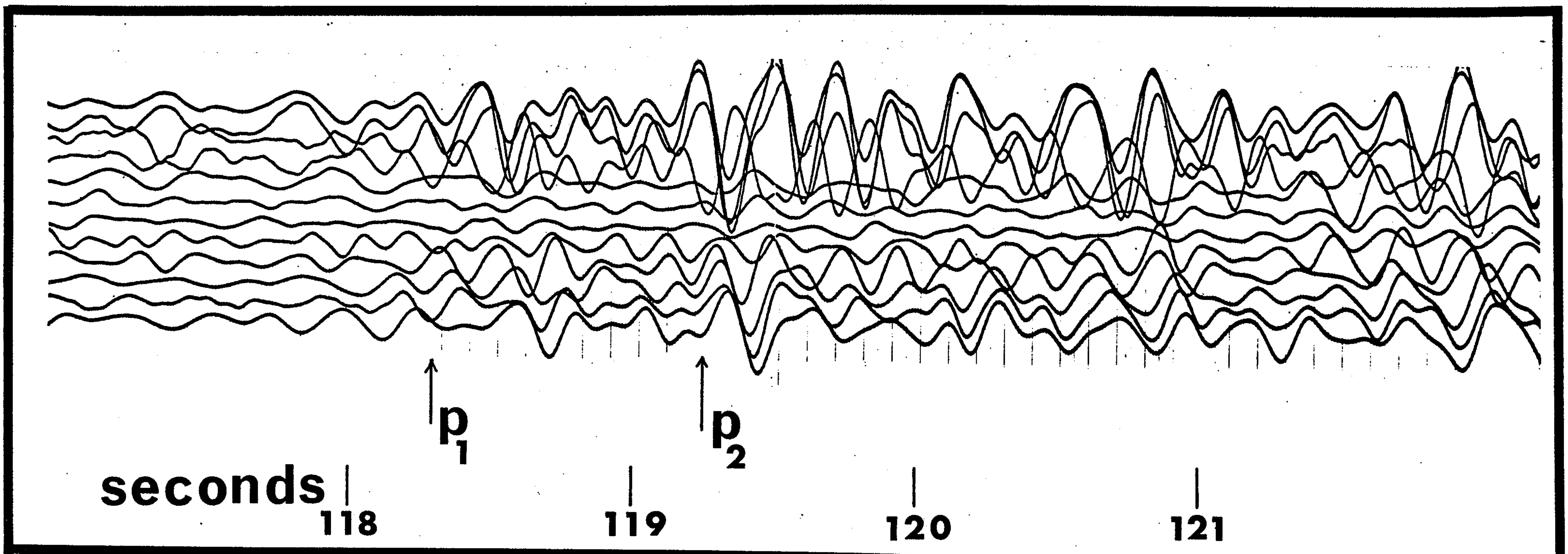

Fig. 11c. Record S3 (Playback). Distance = 898.4 km.

Attenuation (dB)

Channel	1	2	3	4	5	6	7	8	9	10	11	12
Field Record	18	18	18	18	24	24	24	24	24	24	24	24
Playback	48	48	48	48	48	48	48	48	48	48	48	48

Frequency Setting for Field Record = 18 c.p.s. (all channels).

Frequency Setting for Playback = 8 c.p.s. (all channels).

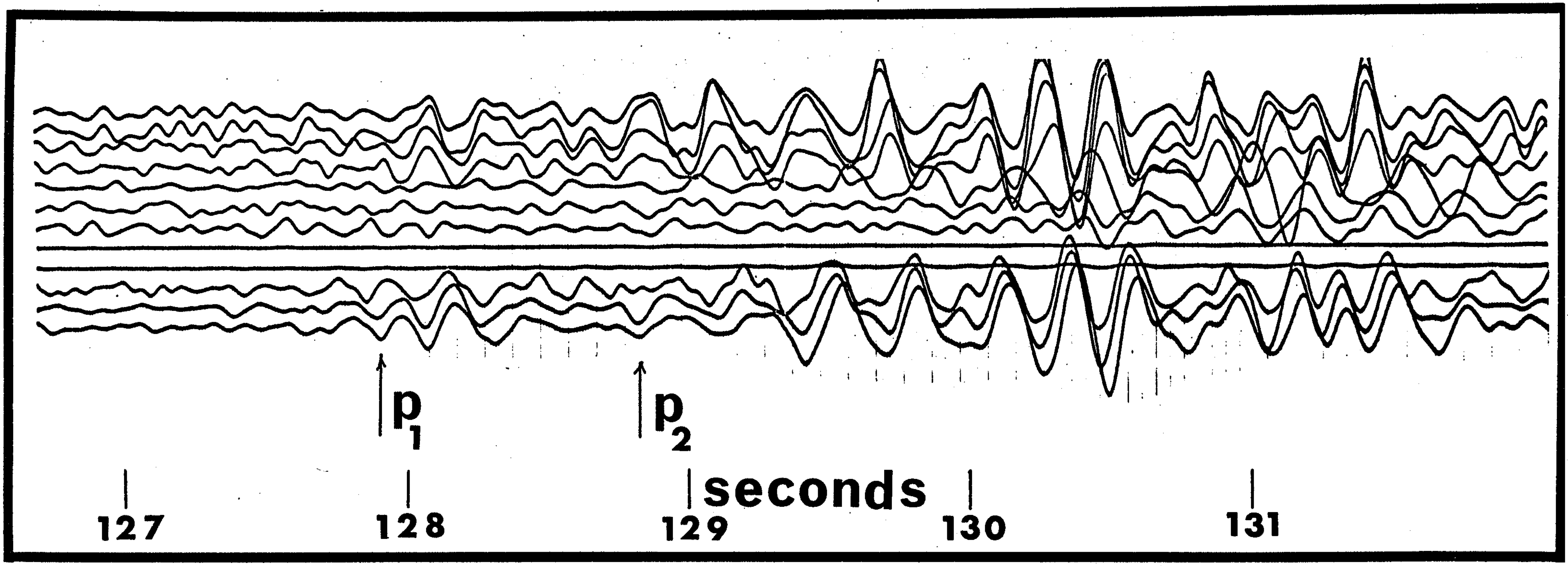

Fig. 11d. Record S4 (Playback). Distance = 979.9 km.

Attenuation (dB)

Channel	1	2	3	4	5	6	7	8	9	10	11	12
Field Record	18	18	18	18	18	18	18	24	24	18	18	18
Playback	48	48	48	48	48	48	48	48	48	48	48	48

Frequency Setting for Field Record = 18 c.p.s. (all channels).

Frequency Setting for Playback = 8 c.p.s. (all channels).

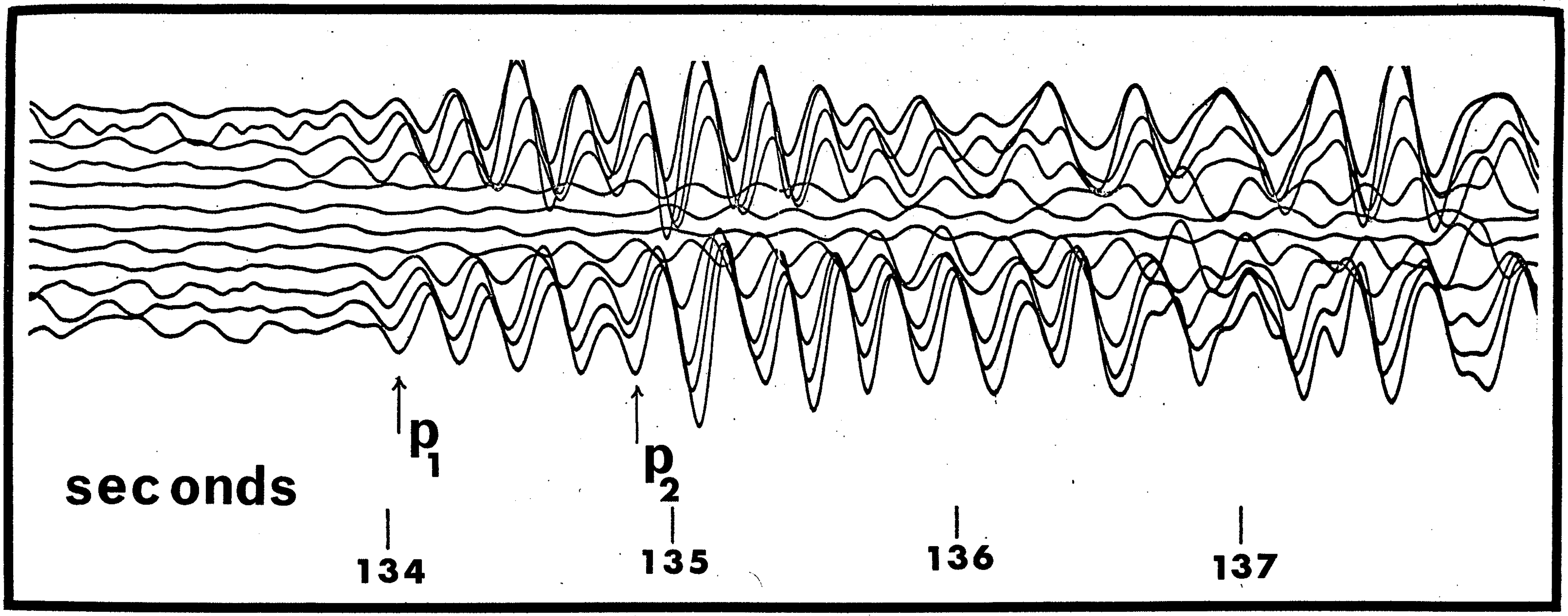

Fig. 11e. Record S5 (Playback). Distance = 1030.4 km.

Attenuation (dB)

Channel	1	2	3	4	5	6	7	8	9	10	11	12
Field Record	24	24	24	24	24	24	24	24	24	24	24	24
Playback	42	42	42	42	48	48	48	48	42	42	42	42

Frequency Setting for Field Record = 18 c.p.s. (all channels).

Frequency Setting for Playback = 8 c.p.s. (all channels).

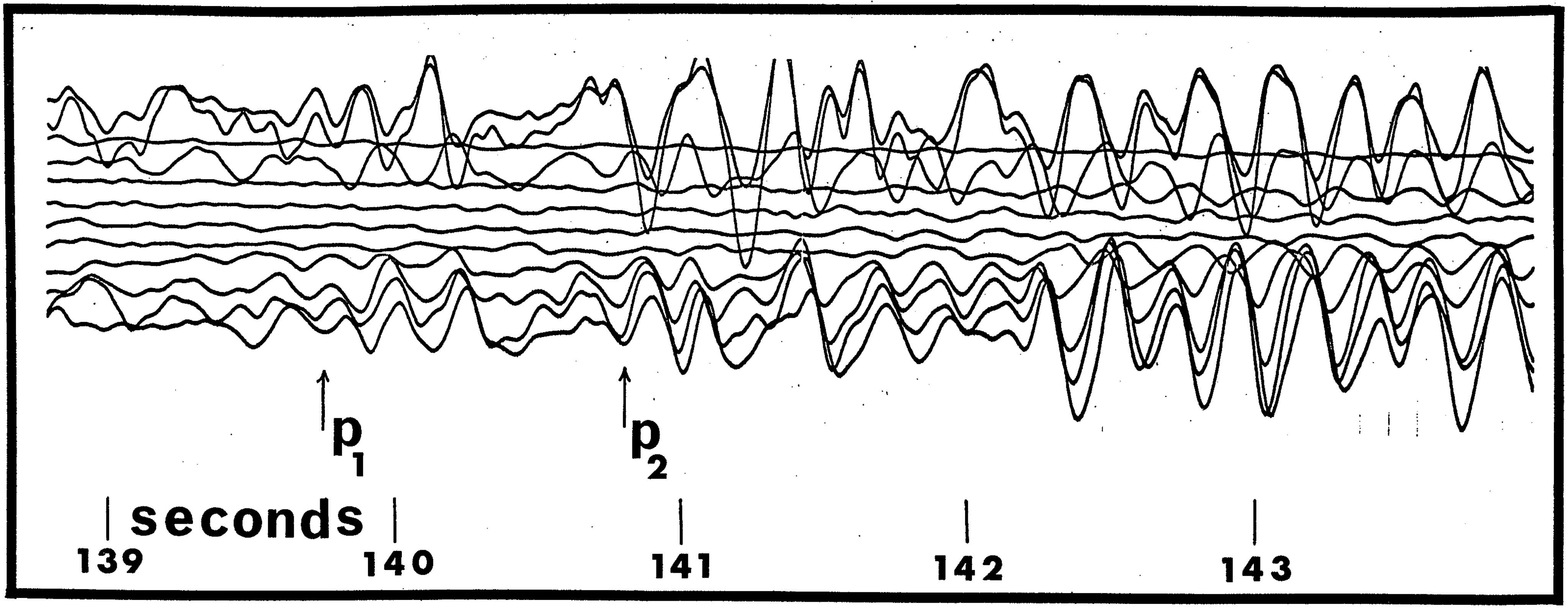

Fig. 11f. Record S6 (Playback). Distance = 1080.6 km.

Attenuation (dB)

Channel	1	2	3	4	5	6	7	8	9	10	11	12
Field Record	30	30	30	30	30	30	30	30	30	30	30	30
Playback	36	36	36	36	48	48	48	48	36	36	36	36

Frequency Setting for Field Record = 18 c.p.s. (all channels).

Frequency Setting for Playback = 8 c.p.s. (all channels).

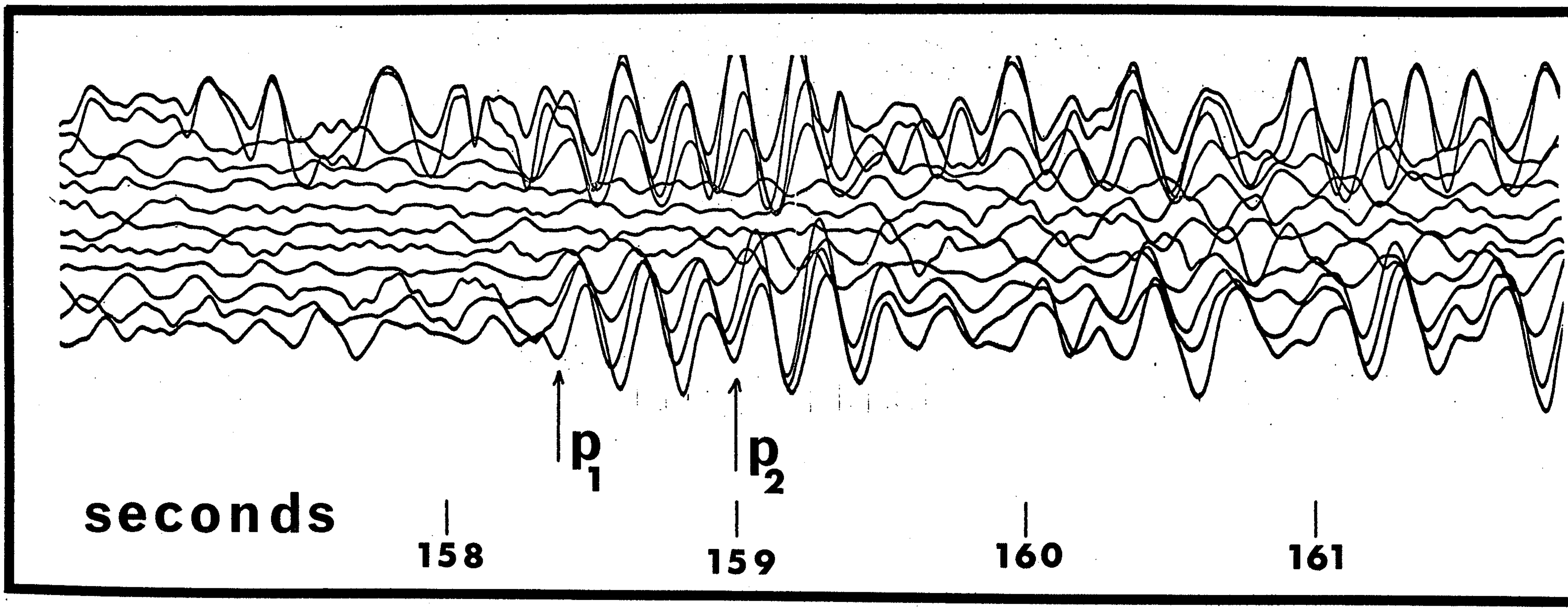

Fig. 11g. Record S7 (Playback). Distance = 1229.4 km.

Attenuation (dB)

Channel	1	2	3	4	5	6	7	8	9	10	11	12
Field Record	18	18	18	18	24	24	24	24	24	24	24	24
Playback	48	48	48	48	48	48	48	48	42	42	42	42

Frequency Setting for Field Record = 18 c.p.s. (all channels).

Frequency Setting for Playback = 8 c.p.s. (all channels).

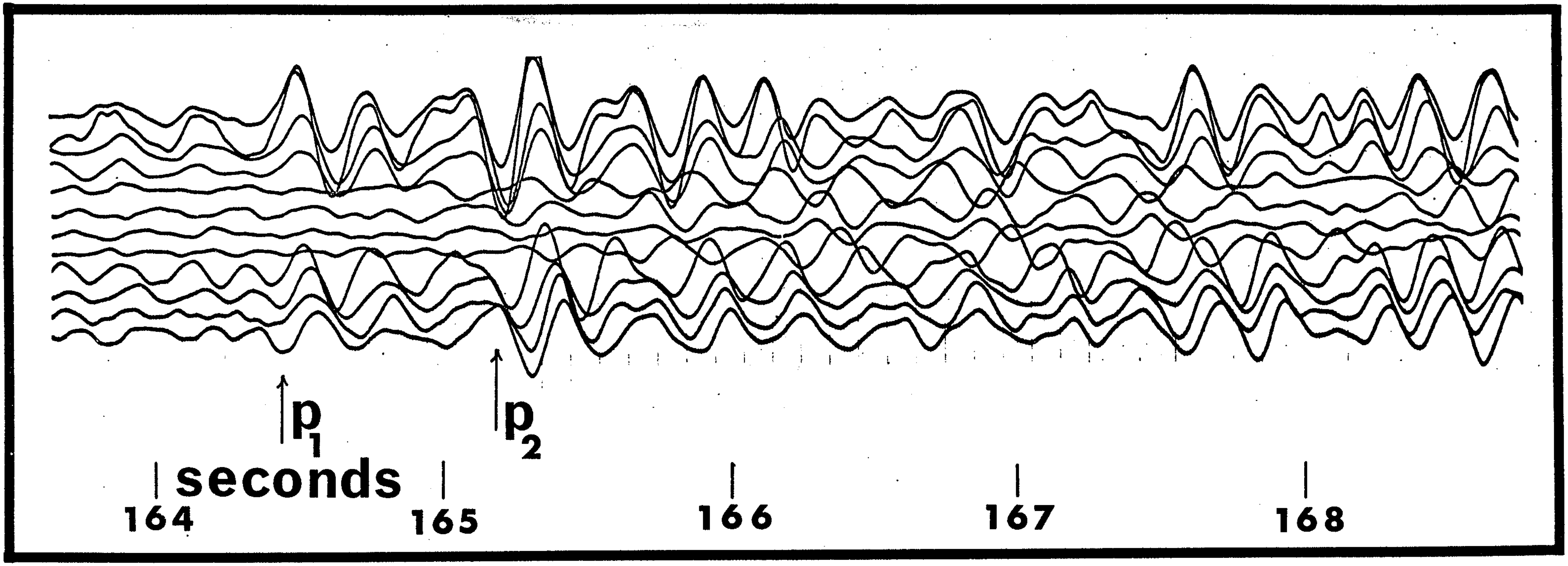

Fig. 11h. Record S8 (Playback). Distance = 1284.3 km.

Attenuation (dB)

Channel	1	2	3	4	5	6	7	8	9	10	11	12
Field Record	24	24	24	24	24	24	24	24	24	24	24	24
Playback	42	42	42	42	48	48	48	48	42	42	42	42

Frequency Setting for Field Record = 18 c.p.s. (all channels).

Frequency Setting for Playback = 8 c.p.s. (all channels).

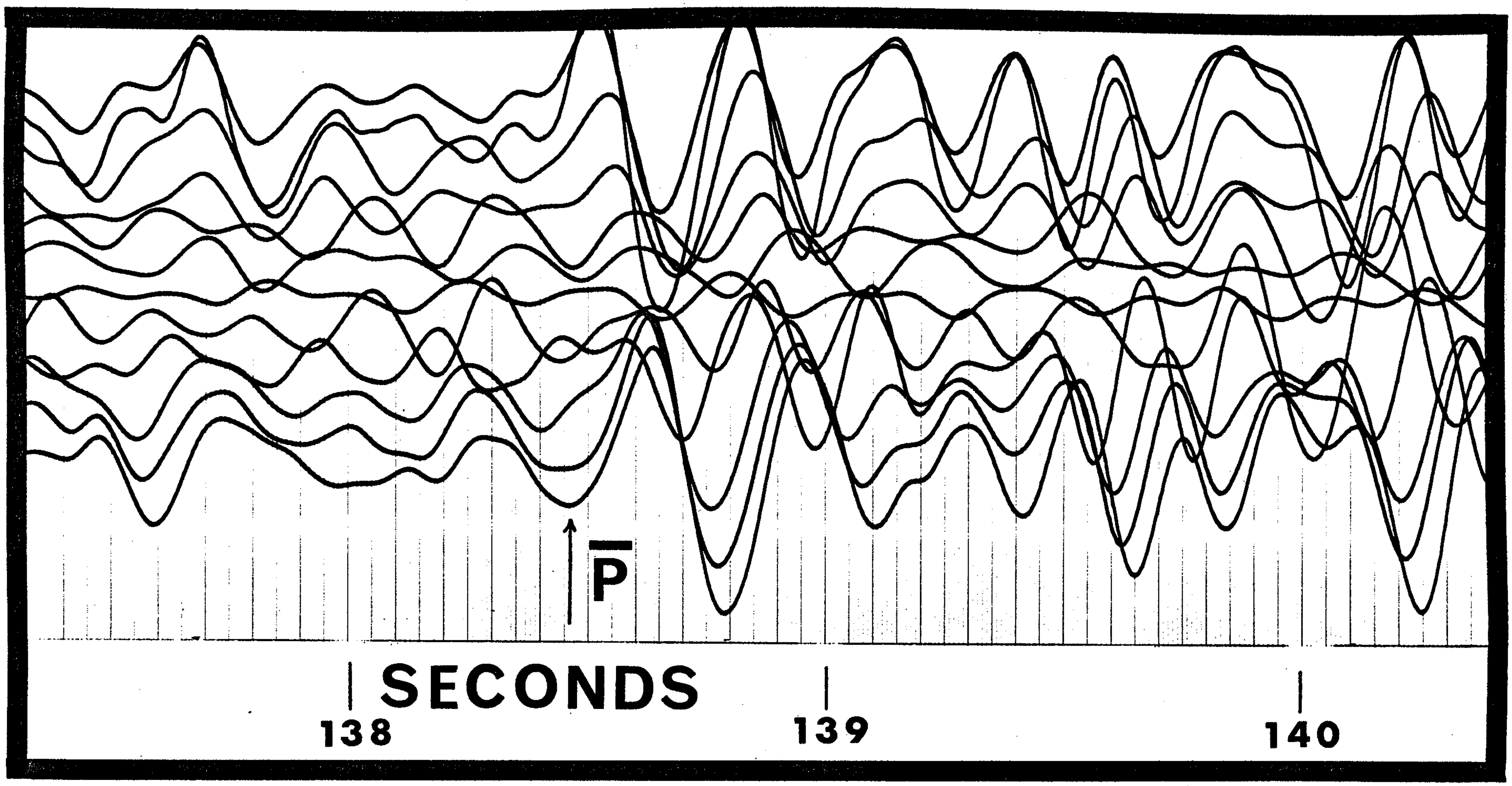

Fig. 12a. $\overline{P}$ Phase Record S2. Distance = 830.6 km.

Attenuation (dB)

Channel	1	2	3	4	5	6	7	8	9	10	11	12
Field Record	30	30	30	30	30	30	30	30	30	30	30	30
Playback	42	42	42	42	42	42	42	42	42	42	42	42

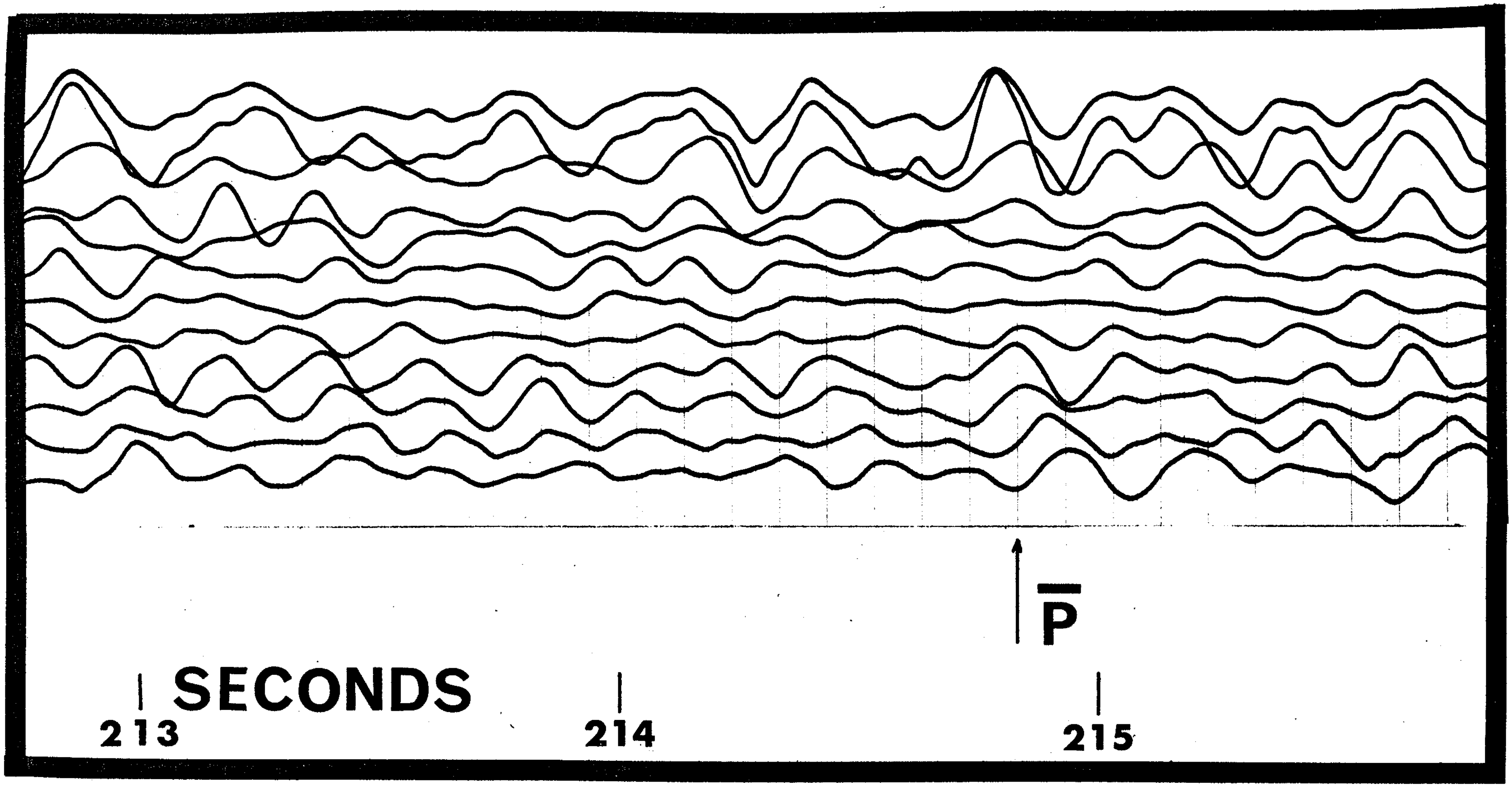

Fig. 12b. $\overline{P}$ Phase, Record S8. Distance = 1284.3 km.

Attenuation (dB)

Channel	1	2	3	4	5	6	7	8	9	10	11	12
Field Record	24	24	24	24	24	24	24	24	24	24	24	24
Playback	42	42	42	42	48	48	48	48	42	42	42	42

Frequency Setting for Field Record = 18 c.p.s. (all channels).

Frequency Setting for Playback = 8 c.p.s. (all channels).

CHAPTER V

CONCLUSIONS

Digital filtering techniques offered no improvement over simple analog playbacks of the seismic records obtained; the VLF-2 system, which is designed for long range refraction experiments, was found to be effective in increasing the signal to noise ratio of the seismic data.

P_1, the first arrival, arrives at times in accordance with a velocity function that increases linearly and slowly with depth below the base of the crust. Uncertainty of crustal structure, however, produces uncertainty in the velocity at the base of crust, V_m, and the velocity gradient within the upper mantle. An average crustal structure for interior plains and plateaux suggests a value of 8.10 ± 0.5 km/sec for V_m, and a gradient between 0 sec^{-1} and about 0.003 sec^{-1}. Arrival times of a second event, P_2, and observed P_2/P_1 amplitude ratios suggest a rapid increase in velocity gradient occurring between depths of about 120 kilometers and 150 kilometers. The incomplete triplication formed by P_1 and P_2 suggests the existence of a zone of low velocity gradient below the rapid increase. Thus, it is not necessary to explain the incomplete triplication by the existence of a low velocity zone.

APPENDIX I

RAY THEORY AND POSITIVE LINEAR VELOCITY-DEPTH GRADIENTS

Travel-time and Distance Equations

It was found that for the distance range of this study the flat earth approximation was inaccurate. The travel time and distance of a ray which travels between radii r_1 and r_2 in a spherically stratified earth are given by Bullen (1963).

$$\Delta = p \int_{r_2}^{r_1} r^{-1} (n^2 - p^2)^{-\frac{1}{2}} \, dr \qquad \ldots \text{ I·1}$$

$$\Delta = \int_{r_2}^{r_1} n^2 r^{-1} (n^2 - p^2)^{-\frac{1}{2}} \, dr \qquad \ldots \text{ I·2}$$

$$p = \frac{r}{V} \sin \alpha \qquad \ldots \text{ I·3}$$

where,

Δ = angular distance travelled by ray

T = travel time of ray

r = distance from center of earth to point on ray path

α = angle between direction of ray path and radius vector

V = velocity (a function of r only)

p = ray parameter (constant for each ray)

n = r/V

An earth model consisting of any number of spherical shells, for which the velocity in the i^{th} shell is given by equation I·4, has been considered.

$$V = m_i r + b_i \qquad \ldots \text{ I·4}$$

where m_i and b_i are constants. For positive velocity-depth gradients, $m_i \leq 0$ and therefore $b_i \geq 0$. The following definitions are useful;

r_i = radial coordinate to the top of the i^{th} shell

V_i = velocity at the top of the i^{th} shell

Δ_i = angular distance travelled by ray through the i^{th} shell

T_i = travel time of ray through the i^{th} shell

From equations I·1, I·2, and I·4, Δ and T for the i^{th} shell are,

$$\Delta_i = 2p \int_{r_{i+1}}^{r_i} r^{-1} \left[\frac{r^2}{(m_i r+b_i)^2} - p^2\right]^{-\frac{1}{2}} dr \qquad \ldots \text{ I·5}$$

$$T_i = 2 \int_{r_{i+1}}^{r_i} \frac{r}{(m_i r+b_i)^2} \left[\frac{r^2}{(m_i r+b_i)^2} - p^2\right]^{-\frac{1}{2}} dr \qquad \ldots \text{ I·6}$$

Stewart (1968) solves equations I·5 and I·6. The following solutions are based on those given by Stewart, but differ in the following way; expressions of the form ln(x) have been changed to ln(|x|). For $m < 0$, the solutions of I·5 and I·6 depend upon the value of $C = 1 - m_i^2 p^2$.

C < 0

$$\frac{\Delta_i}{2} = \left\{\frac{m_i p}{\sqrt{-C}} \arcsin\left[\frac{-Cr}{pb_i} + m_i p\right] + \arcsin\left[-m_i p - \frac{pb_i}{r}\right]\right\}_{r_{i+1}}^{r_i}$$

$$\frac{T_i}{2} = \left\{\frac{-1}{m_i}\left[\frac{1}{\sqrt{-C}} \arcsin\left[\frac{-CV+b_i}{-pm_i b_i}\right] + \ln\left(\left|\frac{-m_i\sqrt{r^2-p^2V^2}+b_i}{V} -1\right|\right)\right]\right\}_{r_{i+1},V_{i+1}}^{r_i,V_i}$$

C = 0

$$\frac{\Delta_i}{2} = \left\{-\sqrt{\frac{-1-2m_i r}{b_i}} + \arcsin\left[1 + \frac{b_i}{m_i r}\right]\right\}_{r_{i+1}}^{r_i}$$

$$\frac{T_i}{2} = \left\{\frac{1}{m_i}\left(\sqrt{\frac{1-2V}{b_i}} + \ln\left(\left|\left(\sqrt{\frac{1-2V}{b_i}} - 1\right)/\left(\sqrt{\frac{1-2V}{b_i}} + 1\right)\right|\right)\right)\right\}_{V_{i+1}}^{V_i}$$

C > 0

$$\frac{\Delta_i}{2} = \left\{\frac{m_i p}{\sqrt{C}} \ln\left(\left|\sqrt{r^2-p^2V^2} +r\sqrt{C} - \frac{m_i b_i p^2}{\sqrt{C}}\right|\right) + \arcsin\left[-m_i p -\frac{pb_i}{r}\right]\right\}_{r_{i+1}, V_{i+1}}^{r_i,V_i}$$

$$\frac{T_i}{2} = \left\{\frac{-1}{m_i\sqrt{C}}\ln\left(\left|-m_i\sqrt{r^2-p^2V^2}+V\sqrt{C}-\frac{b_i}{\sqrt{C}}\right|\right)-\frac{1}{m_i}\ln\left(\left|\frac{-m_i\sqrt{r^2-p^2V^2}+b_i}{V}-1\right|\right)\right\}_{r_{i+1}, V_{i+1}}^{r_i,V_i}$$

When $m_i = 0$, Δ_i and T_i are,

$$\frac{\Delta_i}{2} = \{\arccos[pb_i/r]\}_{r_{i+1}}^{r_i} \qquad \frac{T_i}{2} = \left\{\frac{1}{b_i}\sqrt{r^2-p^2b_i^2}\right\}_{r_{i+1}}^{r_i}$$

For a ray which bottoms in the i^{th} layer, Δ_i and T_i are found from one of the above sets of equations by substituting r_B and V_B for r_{i+1} and V_{i+1}.

r_B = the radial coordinate at the deepest point of penetration.

V_B = velocity at r_B.

The total travel time and distance for a ray which bottoms in the n^{th} spherical shell are:

$$\Delta = \sum_{i=1}^{n} \Delta_i \qquad\qquad T = \sum_{i=1}^{n} T_i$$

Amplitude Ratios (Geometric Spreading)

For an energy source at the earth's surface, the effect of geometric spreading on vertical amplitude is given by (Bullen, 1963),

$$A^2 \propto \frac{I \tan^2 e \sec^2 e (1+3\tan^2 e)^2}{n^2 \sin\Delta (\tan^2 e - \sin^2 e)^{\frac{1}{2}} \{4 \tan e \tan f + (1+3\tan^2 e)^2\}^2} \left|\frac{d^2T}{d\Delta^2}\right| \qquad \text{I·7}$$

where:

A = vertical amplitude at recording site

I = power/unit solid angle at source

e = angle of emergence at recording site

n = r/V at surface

$\cos^2 f = \cos^2 e/3$

Since $d^2T/d\Delta^2 = 1/d\Delta/dp$, A can be calculated for various rays arriving at the same distance; thus, vertical amplitude ratios can be determined.

APPENDIX II

PROGRAM "RAY" DESCRIPTION

1. Identification

   Title: Calculations of time and distance for rays which travel in an earth model consisting of any number of spherical shells, in each of which velocity increases linearly with depth.

   Programmer: Allan Bates

   Date: September, 1970

   Language: Fortran IV

2. Purpose

   To show the effects of spherical shells, in which velocity increases linearly with depth, on the time-distance relation.

3. Usage

   Operational Procedure: The main program reads the input data. Subroutine "Ray" calculates time-distance tables.

   Input Parameters:

   NM = number of models for which tables are to be calculated.

   NN = number of layers + 1 for the models.

(Z(I), I = 1, NN) = depth to the top of the i^{th} layer (kilometers). Z(1) must always be zero.

(VC(I), I = 1, NN-1) = velocity at the top of the i^{th} layer (km/sec).

(M(I), I = 1, NN-1) = linear velocity gradient in the i^{th} layer ($seconds^{-1}$). M(I) must always be less than or equal to zero.

Calculated Parameters

(RC(I), I = 1, NN-1) = distance from centre of earth to top of i^{th} layer (kilometers).

(RD(I), I = 1, NN-1) = distance from center of earth to bottom of i^{th} layer (kilometers).

(VCX(I), I = 1, NN-1) = velocity at the bottom of the i^{th} layer (km/sec).

For each ray, the following values are calculated,

DB = depth at which ray bottoms (kilometers).

RB = distance from center of earth to point at which ray bottoms (kilometers).

VB = velocity at DB (km/sec).

IB = number of layer in which ray bottoms.

(DEL(I), I = 1, IB) = half the distance (degrees) travelled in the i^{th} layer.

(TI), I = 1, IB) = half the travel time in the i^{th} layer (seconds).

DIST = total distance travelled (kilometers).

TIME = total travel time (seconds).

AVEL = apparent velocity of time-distance relation at the distance at which the ray emerges (km/sec).

4. Comments

The program is used for spherical shells for which the velocity, V, in the i^{th} shell is,

$$V = M(I) \times R + B(I) \qquad \text{...II.1}$$

where,

R = distance from center of earth

B(I) = constant (km/sec)

When velocity is expressed as a function of depth, equation (II.1) becomes

$$V = VC(I) - M(I) \times (Z - Z(I)) \qquad \text{...II.2}$$

where Z = depth (kilometers).

Velocity must increase with depth and thus $M(I) \leq 0$.

Equation (II.2) is convenient for determining input parameters. Within the program, equation (I.1) is used for calculations.

Following is an example of "Ray". Calculated values of DB, DIST, and TIME are given in the output. The object program required 36 k bytes of storage space. The central processing unit time for calculations involving over 600 rays was 0.22 min.; 7.34 seconds of this time was used for the compile step.

```
      DOUBLE PRECISION Z(10),VC(9),RC(9),RD(9),VCX(9),B(9),M(9),BN(9),
     1DEL(9),T(9)
```



```
C         PROGRAM RAY COMPUTES TIME-DISTANCE TABLES FOR EARTH
C         MODELS CONSISTING OF ANY NUMBER OF SPHERICAL SHELLS.
C         VELOCITY INCREASES LINEARLY WITH DEPTH
C              INPUT AS FOLLOWS,
C               NM=NUMBER OF MODELS
C               NN=NUMBER OF LAYERS+1
C               (Z(I),I=1,NN)=DEPTH TO TOP OF ITH LAYER
C                             (Z(1) MUST ALWAYS BE ZERO)
C               (VC(I),I=1,NN-1)=VELOCITY AT TOP OF ITH LAYER
C               (M(I),I=1,NN-1)=LINEAR GRADIENT IN ITH LAYER
C                   (M(I) MUST BE LESS THAN OR EQUAL TO ZERO)
C               VELOCITY IN EACH LAYER IS,
C                   V=VC(I)-M(I)*(Z-Z(I)),WHERE,V=VELOCITY,Z=DEPTH
C               OUTPUT,
C                   A TABLE RELATING DEPTH OF PENETRATION,
C                   DISTANCE TRAVELLED,AND TRAVEL TIME
C         THE MAIN PROGRAM READS THE INPUT DATA .CALCULATIONS
C         ARE DONE BY SUBROUTINE RAY
  101 FORMAT(2I5)
  102 FORMAT(5F10.2)
  103 FORMAT(5F10.5)
      READ(5,101) NM,NN
      LL=0
      J=NN-1
      READ(5,102) (Z(I),I=1,NN)
      READ(5,102) (VC(I),I=1,J)
      READ(5,103) (M(I),I=1,J)
 490  CALL RAY(NN,J,Z,VC,RC,RD,VCX,B,M,BN,DEL,T)
      LL=LL+1
      IF(LL.LT.NM) GO TO 490
 96   CONTINUE
      CALL EXIT
      END
```

```
      SUBROUTINE RAY(NN,J,Z,VC,RC,RD,VCX,B,M,BN,DEL,T)
      DOUBLE PRECISION Z(NN),VC(J),RC(NN),RD(J),VCX(J),B(J),M(J),
     1BN(J),RB,VB,P,DB,DEL(J),T(J),A,F,PHI,DIST,TIME,PIE,AVEL,C
C        DEFINITION OF PARAMETERS ,
C             (RC(I),I=1,NN-1)=DISTANCE FROM CENTER OF EARTH
C                              TO TOP OF ITH LAYER
C             (RD(I),I=1,NN-1)=DISTANCE FROM CENTER OF EARTH
C                              TO BOTTOM OF ITH LAYER
C             (VCX(I),I=1,NN-1)=VELOCITY AT THE BOTTOM OF THE
C                               ITH LAYER
C             DB=DEPTH AT WHICH RAY BOTTOMS
C             RB=DISTANCE FROM CENTER OF EARTH TO POINT AT
C                WHICH RAY BOTTOMS
C             VB=VELOCITY AT DB
C             AVEL=APPARENT VELOCITY OF RAY WHICH BOTTOMS AT DB
C             (DEL(I),I=1,NN-1)=HALF CONTRIBUTION OF ITH LAYER
C                               TO DISTANCE.(DEL(I) IS CALCULATED
C                               IN DEGREES)
C             (T(I),I=1,NN-1)=HALF CONTRIBUTION OF ITH
C                             LAYER TO TRAVEL TIME
C             P=CONVENTIONAL RAY PARAMETER (BULLEN ,1963)
C        THE SUBROUTINE USES THE FOLLOWING RELATION FOR VELOCITY
C        IN THE ITH LAYER ,
C             V=M(I)*R+B(I)
C        WHERE R=DISTANCE FROM CENTER OF EARTH
  200 FORMAT(1H ,15X,'NUMBER OF LAYERS =',I3)
  201 FORMAT(1H ,15X,'Z(I)(KM)',10X,'VC(I)(KM/SEC)',10X,'M(I)(1/SEC)')
  202 FORMAT(1H ,/,15X,F8.2, 6X,F13.2,14X,F11.5)
  203 FORMAT(1H ,15X,'PENETRATION(KM)', 8X,'DISTANCE(KM)',10X,'TIME(SEC)
     1')
  204 FORMAT(1H ,10X,F15.2,10X,F12.2,10X,F9.2)
  205 FORMAT(1H ,////)
C        WRITE INPUT DATA
      WRITE(6,200) J
      WRITE(6,201)
      DO 50 I=1,J
      WRITE(6,202) Z(I),VC(I),M(I)
   50 CONTINUE
      WRITE(6,205)
      WRITE(6,203)
C        CALCULATE RADIUS OF EARTH AT 50.75 DEGREES LATITUDE
C             RADIUS OF EARTH=RC(1)
      PIE=3.1415926535897932D0/2.0D0
      A=6378.388D0
      F=1.D0/297.D0
      PHI=(50.75D0*3.1415926535897932D0)/(180.0D0)
      RC(1)=A*(1.D0-F*(DSIN(PHI)*DSIN(PHI))
     1+(5.D0/8.D0)*F*F*(DSIN(2.D0*PHI))*(DSIN(2.D0*PHI)))
C        CALCULATE RC(I),RD(I),VCX(I),B(I)
      DO 20 I=1,J
      RC(I+1)=RC(1)-Z(I+1)
      B(I)=VC(I)-M(I)*RC(I)
      VCX(I)=VC(I)-M(I)*(Z(I+1)-Z(I))
      BN(I)=B(I)/DABS(B(I))
      RD(I)=RC(1)-Z(I+1)
   20 CONTINUE
C        INITIATE VALUE OF RAY PARAMETER
      P=RC(2)/VC(2)+0.049D0
```

```
 10   P=P-0.05D0
C        DETERMINE IF RAY SUFFERS TOTAL REFLECTION. IF RAY IS
C        TOTALLY REFLECTED , THEN IREF=1. OTHERWISE ,IREF=0.
C        ALSO CALCULATE RB AND VB
C        FINAL VALUE OF IB IS NUMBER OF LAYER IN WHICH RAY BOTTOMS
      IREF=0
      DO 1 I=1,J
      IB=I
      IB2=I+1
      RB=(P*B(I))/(1.D0-P*M(I))
      VB=M(I)*RB+B(I)
      IF(RB.GE.RC(I)) GO TO 70
      IF(RB.LE.RC(I).AND.RB.GE.RC(IB2)) GO TO 2
      GO TO 1
 70   RB=RC(I)
      VB=VC(I)
      IREF=1
      IB=IB-1
      WRITE(6,71) IB
 71   FORMAT(1H ,'REF FROM',I3)
      GO TO 2
 1    CONTINUE
 2    DB=RC(1)-RB
      AVEL=VB*RC(1)/RB
C        IF RAY BOTTOMS BELOW REGION OF INTEREST , END CALCULATION
C        FOR PARTICULAR MODEL
      IF(RB.LT.RC(NN)) GO TO 300
      DIST=0.0D0
      TIME=0.0D0
C        FINAL VALUE OF 'DIST' IS TOTAL DISTANCE TRAVELLED
C        FINAL VALUE OF 'TIME' IS TOTAL TRAVEL TIME
C        DO LOOP WHICH CALCULATES DEL(I) AND T(I)
      DO 4 I=1,IB
      C=1.0D0-M(I)*M(I)*P*P
      IF(IREF.EQ.1) GO TO 60
      IF(I.NE.IB) GO TO 60
C        SPECIAL EQUATIONS FOR LAYER IN WHICH RAY BOTTOMS
      IF(M(I).EQ.0.0D0) GO TO 45
      IF(C) 46,47,48
 45   DEL(I)=(DARSIN(-C*RC(I)/(P*DABS(B(I)))+M(I)*P*BN(I)))*M(I)*
     1P/((-C)**.5D0)
     1+(DARSIN(-M(I)*P*BN(I)-P*DABS(B(I))/RC(I)))*BN(I)
     1+(M(I)*P/((-C)**.5D0)+1.D0)*PIE
      T(I)=((DARSIN((-C*VC(I)+B(I))/(P*DABS(M(I)*B(I)))))
     1/((-C)**.5D0)+(DLOG(DABS((DABS(M(I))*((RC(I)*RC(I)-P*P*VC(I)*VC(I
     1))**.5D0)
     1+DABS(B(I)))/(VC(I))-BN(I)))))*BN(I))/DABS(M(I))
     1-(PIE/((-C)**.5D0)+DLOG(DABS(-M(I)*RB/VB)))/DABS(M(I))
      GO TO 9
 47   DEL(I)=-((-1.D0-2.D0*M(I)*RC(I)/B(I))**.5D0)*BN(I)
     1+(DARSIN(-(M(I)*B(I))/(DABS(M(I)*B(I)))
     1-DABS(B(I)/M(I))/RC(I)))*BN(I)+PIE
      T(I)=-((1.D0-2.D0*VC(I)/B(I))**.5D0
     1+DLOG(DABS(((1.D0-2.D0*VC(I)/B(I))**.5D0-1.D0)/
     1((1.D0-2.D0*VC(I)/B(I))**.5D0+1.D0))))*(BN(I)/DABS(M(I)))
      GO TO 9
 48   DEL(I)=(DLOG(DABS((RC(I)*RC(I)-P*P*VC(I)*VC(I))**.5D0
     1+RC(I)*(C**.5D0)-M(I)*B(I)*P*P/(C**.5D0))))*(M(I)*P/
```

```
      1(C**.5D0))+(DARSIN(-M(I)*P*BN(I)-P*DABS(B(I))/RC(I)))
      1*BN(I)-(DLOG(DABS(P*B(I)/(C**.5D0))))*M(I)*P/(C**.5D0)+PIE        75
       T(I)=(DLOG(DABS(DABS(M(I))*((RC(I)*RC(I)-P*P*
      1VC(I)*VC(I))**.5D0)+VC(I)*(C**.5D0)-B(I)/(C**.5D0))))
      1/(DABS(M(I))*(C**.5D0))
      1+(DLOG(DABS((DABS(M(I))*((RC(I)*RC(I)-P*P*VC(I)*VC(I))**.5D0)+
      1DABS(B(I)))/(VC(I))-BN(I))))*(BN(I)/(DABS(M(I))))
      1-(DLOG(DABS(M(I)*P*B(I)/(C**.5D0))))/(DABS(M(I))*(C**.5D0))
      1-(DLOG(DABS(-M(I)*P)))*BN(I)/(DABS(M(I)))
       GO TO 9
   45  DEL(I)=DARCOS(P*B(I)/RC(I))
       T(I)=((RC(I)*RC(I)-P*P*B(I)*B(I))**.5D0)/B(I)
       GO TO 9
C         EQUATIONS FOR LAYERS ABOVE LAYER IN WHICH RAY BOTTOMS
   60  IF(M(I).EQ.0.0D0) GO TO 5
       IF(C) 6,7,8
    6  DEL(I)=(DARSIN(-C*RC(I)/(P*DABS(B(I)))+M(I)*P*BN(I))-
      1DARSIN(-C*RD(I )/(P*DABS(B(I)))+M(I)*P*BN(I)))*M(I)*P/((-C)**.5D0)
      1+(DARSIN(-M(I)*P*BN(I)-P*DABS(B(I))/RC(I))
      1-DARSIN(-M(I)*P*BN(I)-P*DABS(B(I))/RD(I )))*BN(I)
       T(I)=((DARSIN((-C*VC(I)+B(I))/(P*DABS(M(I)*B(I)))))/((-C)**.5D0)
      1+(DLOG(DABS((DABS(M(I))*((RC(I)*RC(I)-P*P*VC(I)*VC(I))**.5D0)
      1+DABS(B(I)))/(VC(I))-BN(I))))*BN(I))/(DABS(M(I)))
      1-((DARSIN((-C*VCX(I)+B(I))/(P*DABS(M(I)*B(I)))))/((-C)**.5D0)
      1+(DLOG(DABS((DABS(M(I))*((RD(I)*RD(I)-P*P*VCX(I)*VCX(I))**.5D0)
      1+DABS(B(I)))/(VCX(I))-BN(I))))*BN(I))/(DABS(M(I)))
       GO TO 9
    7  DEL(I)=-((-1.D0-2.D0*M(I)*RC(I)/B(I))**.5D0)*BN(I)
      1+(DARSIN(-(M(I)*B(I))/(DABS(M(I)*B(I)))
      1-DABS(B(I)/M(I))/RC(I)))*BN(I)
      1+((-1.D0-2.D0*M(I)*RD(I)/B(I))**.5D0)*BN(I)
      1-(DARSIN(-(M(I)*B(I))/(DABS(M(I)*B(I)))-DABS(B(I)/M(I))
      1/RD(I )))*BN(I)
       T(I)=-((1.D0-2.D0*VC(I)/B(I))**.5D0+DLOG(DABS(((1.D0-2.D0*VC(I)/
      1B(I))**.5D0-1.D0)/
      1((1.D0-2.D0*VC(I)/B(I))**.5D0+1.D0))))*(BN(I)/DABS(M(I)))
      1+((1.D0-2.D0*VCX(I)/B(I))**.5D0+
      1DLOG(DABS(((1.D0-2.D0*VCX(I)/B(I))**.5D0-1.D0)
      1/((1.D0-2.D0*VCX(I)/B(I))**.5D0+1.D0))))*(BN(I)/DABS(M(I)))
       GO TO 9
    8  DEL(I)=(DLOG(DABS((RC(I)*RC(I)-P*P*VC(I)*VC(I))**.5D0
      1+RC(I)*(C**.5D0)-M(I)*B(I)*P*P/(C**.5D0)))
      1-DLOG(DABS((RD(I)*RD(I)-P*P*VCX(I)*VCX(I))**.5D0
      1+RD(I)*(C**.5D0)-M(I)*B(I)*P*P/(C**.5D0))))*(M(I)*P/(C**.5D0))
      1+(DARSIN(-M(I)*P*BN(I)-P*DABS(B(I))/RC(I))
      1-DARSIN(-M(I)*P*BN(I)-P*DABS(B(I))/RD(I )))*BN(I)
       T(I)=(DLOG(DABS(DABS(M(I))*((RC(I)*RC(I)-P*P*VC(I)*VC(I))**.5D0)+
      1VC(I)*(C**.5D0)-B(I)/(C**.5D0)))
      1-DLOG(DABS(DABS(M(I))*((RD(I)*RD(I)-P*P*VCX(I)*VCX(I))**.5D0)+
      1VCX(I)*(C**.5D0)-B(I)/(C**.5D0))))/(DABS(M(I))*(C**.5D0))
      1+(DLOG(DABS((DABS(M(I))*((RC(I)*RC(I)-P*P*VC(I)*VC(I))**.5D0)
      1+DABS(B(I)))/(VC(I))-BN(I)))
      1-DLOG(DABS((DABS(M(I))*((RD(I)*RD(I)-P*P*VCX(I)*VCX(I))**.5D0)
      1+DABS(B(I)))/(VCX(I))-BN(I))))*(BN(I)/(DABS(M(I))))
       GO TO 9
    5  DEL(I)=DARCOS(P*B(I)/RC(I))-DARCOS(P*B(I)/RD(I ))
       T(I)=((RC(I)*RC(I)-P*P*B(I)*B(I))**.5D0
      1-(RD(I )*RD(I )-P*P*B(I)*B(I))**.5D0)/B(I)
```

```
 9    DIST=DIST+RC(1)*DEL(I)*2.D0
      TIME=TIME+T(I)*2.D0
      IF(I.NE.IB) GO TO 500
C        WRITE DEPTH OF PENETRATION OF RAY ,DISTANCE TRAVELLED
C        BY RAY AND TRAVEL TIME OF RAY
      WRITE(6,204) DB,DIST,TIME
 500  CONTINUE
 4    CONTINUE
      GO TO 10
 300  CONTINUE
      RETURN
      END
```

NUMBER OF LAYERS = 2

Z(I)(KM)	VC(I)(KM/SEC)	M(I)(1/SEC)
0.0	6.34	0.0
41.06	8.10	-0.00170

PENETRATION(KM)	DISTANCE(KM)	TIME(SEC)
41.06	111.51	21.78
41.24	165.26	28.37
41.41	190.71	31.49
41.59	210.30	33.90
41.76	226.82	35.92
41.93	241.39	37.71
42.11	254.57	39.33
42.28	266.69	40.81
42.46	277.98	42.20
42.63	288.58	43.50
42.80	298.60	44.72
42.98	308.14	45.89
43.15	317.26	47.01
43.33	326.00	48.08
43.50	334.41	49.11
43.68	342.53	50.11
43.85	350.38	51.07
44.02	357.99	52.00
44.20	365.38	52.91
44.37	372.57	53.79
44.55	379.57	54.65
44.72	386.40	55.48
44.89	393.07	56.30
45.07	399.59	57.10
45.24	405.97	57.88
45.42	412.22	58.65
45.59	418.34	59.40
45.77	424.35	60.13
45.94	430.25	60.85
46.12	436.05	61.56
46.29	441.74	62.26
46.46	447.34	62.95
46.64	452.85	63.62
46.81	458.28	64.28
46.99	463.63	64.94
47.16	468.90	65.58
47.34	474.09	66.22
47.51	479.21	66.85
47.69	484.26	67.46
47.86	489.25	68.07
48.03	494.18	68.68
48.21	499.04	69.27
48.38	503.85	69.86
48.56	508.59	70.44
48.73	513.29	71.02
48.91	517.93	71.58
49.08	522.52	72.14
49.26	527.06	72.70
49.43	531.55	73.25
49.61	536.00	73.79
49.78	540.40	74.33
49.95	544.76	74.86

61.86	778.56	103.39
62.04	781.40	103.74
62.21	784.24	104.08
62.39	787.06	104.42
62.56	789.87	104.77
62.74	792.67	105.11
62.92	795.46	105.45
63.09	798.23	105.78
63.27	801.00	106.12
63.44	803.76	106.46
63.62	806.50	106.79
63.79	809.24	107.12
63.97	811.96	107.45
64.14	814.68	107.78
64.32	817.38	108.11
64.50	820.08	108.44
64.67	822.76	108.77
64.85	825.44	109.09
65.02	828.10	109.42
65.20	830.76	109.74
65.38	833.41	110.06
65.55	836.04	110.38
65.73	838.67	110.70
65.90	841.29	111.02
66.08	843.90	111.34
66.25	846.50	111.65
66.43	849.09	111.97
66.61	851.68	112.28
66.78	854.25	112.60
66.96	856.82	112.91
67.13	859.37	113.22
67.31	861.92	113.53
67.49	864.46	113.84
67.66	867.00	114.14
67.84	869.52	114.45
68.01	872.04	114.76
68.19	874.55	115.06
68.37	877.05	115.36
68.54	879.54	115.67
68.72	882.03	115.97
68.89	884.50	116.27
69.07	886.97	116.57
69.25	889.44	116.87
69.42	891.89	117.17
69.60	894.34	117.46
69.77	896.78	117.76
69.95	899.21	118.06
70.13	901.64	118.35
70.30	904.06	118.64
70.48	906.47	118.94
70.65	908.87	119.23
70.83	911.27	119.52
71.01	913.66	119.81
71.18	916.04	120.10
71.36	918.42	120.39
71.54	920.79	120.67
71.71	923.16	120.96
71.89	925.51	121.25
72.06	927.86	121.53
72.24	930.21	121.82
72.42	932.55	122.10
72.59	934.88	122.38
72.77	937.20	122.66
72.95	939.52	122.94
73.12	941.83	123.23

50.30	553.35	75.91
50.48	557.58	76.43
50.65	561.78	76.94
50.83	565.94	77.45
51.00	570.06	77.96
51.18	574.14	78.46
51.35	578.20	78.95
51.53	582.21	79.44
51.70	586.20	79.93
51.88	590.15	80.41
52.05	594.07	80.89
52.23	597.96	81.37
52.40	601.82	81.84
52.58	605.65	82.30
52.75	609.45	82.77
52.93	613.22	83.23
53.10	616.97	83.69
53.28	620.69	84.14
53.45	624.38	84.59
53.63	628.04	85.04
53.80	631.69	85.48
53.98	635.30	85.93
54.15	638.90	86.36
54.33	642.47	86.80
54.50	646.01	87.23
54.68	649.54	87.66
54.85	653.04	88.09
55.03	656.52	88.52
55.20	659.97	88.94
55.38	663.41	89.36
55.55	666.83	89.77
55.73	670.22	90.19
55.90	673.60	90.60
56.08	676.96	91.01
56.25	680.29	91.42
56.43	683.61	91.82
56.60	686.91	92.22
56.78	690.19	92.62
56.95	693.46	93.02
57.13	696.70	93.42
57.30	699.93	93.81
57.48	703.14	94.20
57.65	706.34	94.59
57.83	709.51	94.98
58.00	712.67	95.36
58.18	715.82	95.75
58.35	718.95	96.13
58.53	722.06	96.51
58.70	725.16	96.89
58.88	728.25	97.26
59.05	731.32	97.64
59.23	734.37	98.01
59.41	737.41	98.38
59.58	740.43	98.75
59.76	743.45	99.11
59.93	746.44	99.48
60.11	749.43	99.84
60.28	752.40	100.20
60.46	755.36	100.56
60.63	758.30	100.92
60.81	761.23	101.28
60.98	764.15	101.64
61.16	767.05	101.99
61.34	769.95	102.34
61.51	772.83	102.69
61.69	775.70	103.04

LIST OF REFERENCES

ANSTEY, N.A. and NEWMAN, P. 1966. The sectional auto-correlogram and the sectional retro-correlogram. Geophysical Prospecting, vol. 14, No. 4, pp. 389-426.

BARR, K.G. 1967. Upper mantle structure in Canada from seismic observations using chemical explosions. Canadian Journal of Earth Sciences, vol. 4, No. 5.

BULLEN, K.E. 1963. Introduction to the theory of seismology, 3rd edition. University Press, Cambridge.

BURGESS, P. 1969. A study of processing time and storage requirements for digital processing of seismic data. M.Sc. Thesis. Institute of Computer Science, University of Manitoba.

DOBRIN, M.B., INGALLS, A.L. and LONG, J.A. 1965. Velocity and frequency filtering of seismic data using laser light (optical processing spectrum analysis). Geophysics, vol. 30, No. 6, pp. 1144-1178.

DOBRIN, M.B. and FITTON, J.C. 1967. Optical processing and interpretation (Reefs frequency filtering data-enhancement faulting reverberation). vol. 32, No. 5, pp. 801-818.

EMBREE, P., BURG, J.P. and BACKUS, M.M. 1963. Wide-band velocity filtering. The pie-slice process. Geophysics, vol. 28, No. 6, pp. 948-974.

GALBRAITH, J.N., Jr. and WIGGINS, R.A. 1968. Characteristics of optimum multichannel stacking filters (least squares). Geophysics, vol. 33, No. 1, pp. 36-48.

GOUPILLAUD, P.L. 1961. An approach to inverse filtering of near-surface layer effects from seismic records. Geophysics, vol. 26, No. 6, pp. 754-760.

GREEN, R.W.E. and HALES, A.L. 1968. The travel times of P waves to 30° in the central United States and upper mantle structure. Bull. Seism. Soc. Am., vol. 58, No. 1, pp. 267-289.

GREEN, R. and STEINHART, J.S. 1962. On crustal structure deduced from seismic time-distance curves. New Zealand

Journal of Geology and Geophysics, vol. 5, No. 4, pp. 579-591.

GURBUZ, B. 1969. Structure of the earth's crust and upper mantle under a portion of Canadian Shield deduced from travel times and spectral amplitudes of body waves using data from Project Early Rise. Ph.D. Thesis, Dept. of Earth Sciences, University of Manitoba.

HAJNAL, Z. 1970. A continuous deep-crustal seismic refraction and near-vertical reflection profile in the Canadian Shield interpreted by digital processing techniques. Ph.D. Thesis, Dept. of Earth Sciences, University of Manitoba.

HALL, D.H. and BRISBIN, W.C. 1965. Crustal structure from converted head waves in central western Manitoba. Geophysics, vol. 30, No. 6, pp. 1053-1067.

HAMMOND, J.W. 1962. Ghost elimination from reflection records. Geophysics, vol. 27, No. 1, pp. 48-60.

HOLZMAN, M. 1963. Chebyshev optimized geophone arrays. Geophysics, vol. 28, No. 2, pp. 145-155.

INTERNATIONAL DICTIONARY OF GEOPHYSICS, 1967. General Editor, K. Runcorn, Pergamon Press, Library of Congress Catalogue Card No. 66-16369.

JULIAN, B.R. and ANDERSON, D.L. 1968. Travel times apparent velocities and amplitudes of body waves. Bull. Seism. Soc. Am., vol. 58, No. 1, pp. 339-366.

LINDSEY, J.P. 1960. Elimination of seismic ghost reflections by means of a linear filter. Geophysics, vol. 25, No. 1, pp. 130-140.

MAYNE, W.H. 1962. Common reflection point horizontal data stacking techniques. Geophysics, vol. 27, No. 6, pp. 927-938.

McCAMY, K., MEYER, R.P. and SMITH, T.J. 1962. Generally applicable solutions of Zoeppritz' amplitude equations. Bull. Seism. Soc. Am., vol. 52, No. 4, pp. 923-955.

McCONNEL, R.K., Jr. and McTAGGART-COWAN, G.H. 1963. Crustal seismic refraction profiles (a compilation). Institute of Earth Sciences, University of Toronto, Scientific Report, No. 8, Contract No. AF 19 (628)-22.

MEYERHOFF. H.J. 1966. Horizontal stacking and multichannel filtering applied to common depth point seismic data.

Geophysical Prospecting, vol. 14, No. 4, pp. 441-454.

RICE, R.B. 1962. Inverse convolution filters. Geophysics, vol. 27, No. 1, pp. 4-18.

ROBINSON, E.A. 1967. Multichannel time series analysis with digital computer programs. Holden-Day, Inc., San Francisco.

RODEN, R.B. 1965. Horizontal and vertical arrays for teleseismic signal enhancement - detection (vela uniform). Geophysics, vol. 30, No. 4, pp. 597-608.

SÇHEIDER, W.A., PRINE, E.R., Jr. and GILES, B.F. 1965. A new data processing technique for multiple attenuation exploiting differential normal movement. Geophysics, vol. 30, pp. 348-362.

SCHWIND, J.J., BERG, J.W., Jr. and COOK, K.L. 1960. PS converted waves from large explosions. J. Geophys. Res., vol. 65, No. 11, pp. 3817-3824.

SENGBUSH, R.L. and FOSTER, M.R. 1968. Optimum multichannel velocity filters (Wiener). Geophysics, vol. 33, No. 1, pp. 11-35.

SHANKS, J.L., TREITEL, S. and FRASIER, C.W. 1967. Some aspects of fan filtering. Geophysics, vol. 32, No. 5, pp. 789-800.

SILVERMAN, D., LASH, C.C. and HADLEY, C.F. 1963. Murac, a multiple reflection analog computer. Geophysics, vol. 28, No. 6, pp. 990-1000.

STEWART, S.W. 1968. Crustal structure in Missouri by seismic-refraction methods. Bull. Seism. Soc. Am., vol. 58, No. 1, pp. 291-323.

WIENER, N. 1949. Time series. 1.95 (pap. ISPN 0-262-73005-7) MIT Pr.

WHITE, J.E. 1964. Motion product seismograms (detector noise three component geophone) Geophysics, vol. 29, No. 2, pp. 288-298.

WHITE, W.R.H. and SAVAGE, J.C. 1965. A seismic refraction and gravity study of the earth's crust in British Columbia. Bull. Seism. Soc. Am., vol. 55, No. 2, pp. 463-486.